

BRNO UNIVERSITY OF TECHNOLOGY

Faculty of Electrical Engineering
and Communication

BACHELOR'S THESIS

Brno, 2020

Hadi Abdallah



BRNO UNIVERSITY OF TECHNOLOGY

VYSOKÉ UČENÍ TECHNICKÉ V BRNĚ

FACULTY OF ELECTRICAL ENGINEERING AND COMMUNICATION

FAKULTA ELEKTROTECHNIKY
A KOMUNIKAČNÍCH TECHNOLOGIÍ

DEPARTMENT OF ELECTRICAL POWER ENGINEERING

ÚSTAV ELEKTROENERGETIKY

POWER TO GAS

POWER TO GAS

BACHELOR'S THESIS

BAKALÁŘSKÁ PRÁCE

AUTHOR

AUTOR PRÁCE

Hadi Abdallah

SUPERVISOR

VEDOUCÍ PRÁCE

Ing. Lukáš Radil, Ph.D.

BRNO 2020

Bakalářská práce

bakalářský studijní program **Silnoproudá elektrotechnika a elektroenergetika**

Ústav elektroenergetiky

Student: Hadi Abdallah

ID: 203497

Ročník: 3

Akademický rok: 2019/20

NÁZEV TÉMATU:

Power to gas

POKYNY PRO VYPRACOVÁNÍ:

Práce se zabývá jednou ze základních možností akumulace elektrické energie ve formě syntetického metanu - P2G. Student provede analýzu současného stavu a provede matematický model tohoto systému v OpenModelice.

DOPORUČENÁ LITERATURA:

podle pokynů vedoucího práce

Termín zadání: 3.2.2020

Termín odevzdání: 10.6.2020

Vedoucí práce: Ing. Lukáš Radil, Ph.D.

doc. Ing. Petr Toman, Ph.D.
předseda rady studijního programu

UPOZORNĚNÍ:

Autor bakalářské práce nesmí při vytváření bakalářské práce porušit autorská práva třetích osob, zejména nesmí zasahovat nedovoleným způsobem do cizích autorských práv osobnostních a musí si být plně vědom následků porušení ustanovení § 11 a následujících autorského zákona č. 121/2000 Sb., včetně možných trestněprávních důsledků vyplývajících z ustanovení části druhé, hlavy VI. díl 4 Trestního zákoníku č.40/2009 Sb.

ABDALLAH, Hadi. Power to gas. Brno, 2020. Bakalářská práce. Vysoké učení technické v Brně, Fakulta elektrotechniky a komunikačních technologií, Ústav elektroenergetiky. Vedoucí práce Lukáš Radil.

„Prohlašuji, že svou bakalářskou práci na téma Power to gas jsem vypracoval samostatně pod vedením vedoucího bakalářské práce a s použitím odborné literatury a dalších informačních zdrojů, které jsou všechny citovány v práci a uvedeny v seznamu literatury na konci práce. Jako autor uvedené bakalářské práce dále prohlašuji, že v souvislosti s vytvořením této bakalářské práce jsem neporušil autorská práva třetích osob, zejména jsem nezasáhl nedovoleným způsobem do cizích autorských práv osobnostních a jsem si plně vědom následků porušení ustanovení § 11 a následujících autorského zákona č. 121/2000 Sb., včetně možných trestněprávních důsledků vyplývajících z ustanovení části druhé, hlavy VI. díl 4 Trestního zákoníku č. 40/2009 Sb.“

V Brně dne:

.....

ABSTRACT

This thesis deals with power-to-gas; an energy storage technology that converts excess electricity produced by renewable energy sources to synthetic natural gas. The objective was to present the current status of this technology and to create a power-to-gas model in OpenModelica. In addition to a detailed description of each part of the system, the model with simulation results and analysis are presented.

KEY WORDS:

Energy storage; hydrogen; carbon dioxide; methanation; power-to-gas; SNG

ABSTRAKT

Tato práce se zabývá problematikou technologie power-to-gas, která slouží k akumulaci energie tím, že přeměňuje přebytečnou elektrickou energii vyráběnou z obnovitelných zdrojů energie na syntetický zemní plyn. Cílem bylo představit aktuální trendy v oblasti power-to-gas a vytvořit model tohoto systému v OpenModelica.

V práci jsou uvedeny všechny hlavní části systému power-to-gas: výroba elektrické energie, výroba vodíku elektrolýzou, zachycování a separace uhlíku, Sabatierova reakce a typy metanizace. Nejprve byl modelován denní průběh slunečního záření. Poté byl zpracován submodel přeměny záření na elektrickou energii pomocí FV panelů. Dále byl zpracován střídač DC/AC, distribuční cesta a měnič AC/DC pro napájení elektrolyzérů. Stěžejní částí práce bylo zpracování vlastní metanizační jednotky.

Reakce je řešena pomocí van der Waalsovy rovnice reálných plynů. Podle toho je stanovena produkce metanu, který je poté skladován v nádržích. Dále se provádí simulace se dvěma cestami. Za prvé, energie získaná z fotovoltaické elektrárny je přímo vedena přes distribuční soustavu k elektrolyzérům. Za druhé, energie získaná z fotovoltaické elektrárny je přiváděna do 22 kV distribuční sítě, která pak napájí zbytek procesu.

Závěrem práce je zhodnocení, které porovnává celkovou efektivitu systému vzhledem k power-to-gas vůči akumulátorovému úložišti energie.

KLÍČOVÁ SLOVA:

Skladování energie; vodík; oxid uhličitý; metanizace; power-to-gas; SNG

ACKNOWLEDGEMENT

I would like to thank my supervisor Ing. Lukáš Radil, Ph.D, for the great help, guidance, encouragement and advice he has provided throughout my work on this thesis.

Contents

1	Introduction	15
1.1	Power-to-Gas preview:	17
2	Hydrogen supply	18
2.1	Properties	18
2.2	Production	18
2.3	Water electrolysis	19
2.3.1	Alkaline electrolysis	19
2.3.2	Polymer electrolyte membrane electrolysis	20
2.3.3	Solid oxide electrolysis	21
2.4	Hydrogen transport	22
2.4.1	Compressed gas cylinder	22
2.4.2	Cryogenic liquid	22
2.4.3	Pipelines	22
3	Carbon Dioxide Sources	23
3.1	CO ₂ from combustion processes in power plants.	24
3.1.1	CO ₂ capture	24
3.1.2	CO ₂ separation technologies	25
3.1.3	Energy penalty in CCUS	27
3.2	CO ₂ from industrial processes	27
3.3	CO ₂ captured from the atmosphere	28
3.4	CO ₂ transport	28
4	Methanation	29
4.1	Thermodynamics	29
4.2	Effects of pressure, temperature and H ₂ : CO ₂ ratios	29
4.3	H ₂ –CO ₂ separation and recycle	31
4.4	Catalytic methanation	31
4.4.1	Adiabatic fixed-bed reactors	32
4.4.2	Fluidized-bed reactors	32
4.4.3	Three-phase reactors	33
4.4.4	Structured micro-reactors	33
4.4.5	Catalyst and reactor requirements	34
4.5	Biological methanation	35
4.5.1	Biological methanation in a separate reactor	35
4.5.2	In situ biological methanation	36
4.6	Methanation parameters	36
4.6.1	Tolerance of impurities	36
4.6.2	Load change	36
4.6.3	Shutdown	37

4.6.4	Wobbe index	37
5	Openmodelica	38
6	Modelling	39
6.1	Electricity generation	39
6.1.1	Photovoltaic power plant	39
6.1.2	DC/AC inverter	41
6.1.3	Distribution and connection to the power grid	41
6.1.4	Rectification	43
6.2	Electrolysis	44
6.3	Methanation	44
6.3.1	Methanation reaction	44
6.3.2	Van der Waals equation	46
6.3.3	Methane production and storage	47
6.4	Simulation	49
6.5	Energy storage in batteries	57
7	Conclusion	62

List of Figures

1-1	Global energy consumption [Mtoe], 2010 – 2018 [2]	15
1-2	Classification of energy storage technologies by the form of stored energy [5]	16
1-3	Power-to-gas	17
2-1	Alkaline electrolysis [15]	20
2-2	Polymer electrolyte membrane electrolysis [15]	20
2-3	Solid oxide electrolysis [15]	21
3-1	Different CO ₂ sources with their relevant concentrations [18]	23
3-2	Post-combustion capture [21]	24
3-3	Pre-combustion capture [21]	25
3-4	Oxyfuel capture [21]	25
3-5	CO ₂ separation technologies [22]	26
3-6	CO ₂ emission intensity with and without carbon capture [24]	27
4-1	Effects of pressure and temperature with H ₂ /CO ₂ = 4 on CO ₂ methanation: (a) CO ₂ conversion, (b) CH ₄ selectivity, and (c) CH ₄ yield [30]	30
4-2	CH ₄ content at different CO ₂ conversion rates [7]	30
4-3	Molar gas composition at various stages [31]	31
4-4	Catalytic fixed-bed reactors A)Adiabatic fixed-bed reactor; B)Multi-tubular fixed-bed reactor [32]	32
4-5	Fluidized-bed reactor [34]	33
4-6	Three-phase reactor [34]	33
4-7	Structured micro-reactors [35]	34
4-8	Biological methanation in a separate reactor [7]	35
4-9	In situ biological methanation [7]	36
5-1	OpenModelica Connection Editor (OME) modelling [37]	38
5-2	OME plotting [37]	38
6-1	Overall power-to-gas model	39
6-2	Irradiance	39
6-3	PV power plant model	40
6-4	IV curve of a solar cell [39]	41
6-5	Distribution model	42
6-6	Rectification model	43
6-7	Methanation model	45
6-8	Van der Waals equation model	47
6-9	Simulation parameters	49
6-10	Generated power	50
6-11	DC current	51
6-12	Hydrogen production	51
6-13	Methane production	52
6-14	Methane accumulation	52
6-15	Active power from 22 kV MV network	54

6-16 DC current	55
6-17 Hydrogen production	55
6-18 Methane production	56
6-19 Methane accumulation	56
6-20 Batteries model	57
6-21 Batteries model	58
6-22 Simulation parameters	58
6-23 DC current	59
6-24 State of charge (SOC)	59
6-25 Energy	60
6-26 DC current	60
6-27 State of charge (SOC)	61
6-28 Energy	61

List of Tables

2-1	Basic properties of hydrogen [11]	18
2-2	Comparison of parameters of AEC, PEMEC, and SOEC [7]	21
6-1	SHARP - NU-S5 (E3E)-185W parameters at STC [38]	40

Acronym	Description
AEC	Alkaline Electrolysis
CCUS	Carbon Capture Utilization and Storage
CSTR	Continuous Stirred-tank Reactor
CGH ₂	Compressed hydrogen gas
LH ₂	Liquid hydrogen gas
MPP	Maximum Power Point
MV	Medium voltage
MtCO ₂	Million tonnes of carbon dioxide equivalent
Mtoe	Million tonnes of oil equivalent
Nm ³	Normal cubic meter
ppm	parts per million
PEMEC	Polymer Electrolyte Membrane Electrolysis
SOEC	Solid Oxide Electrolysis
SNG	Synthetic Natural Gas
STP	Standard temperature and pressure
STC	Standard testing conditions

Symbol	Description	Unit
F_{V,CH_4}	Volumetric Stream	m^3/h
GHSV	Gas Hourly Space Velocity	h^{-1}
H_{H_2,H_2O}	Henry's law coefficient for Hydrogen in Water	$bar \cdot l/mol$
H_{CO_2,H_2O}	Henry's law coefficient for Carbon Dioxide in Water	$bar \cdot l/mol$
MFR	Methane Formation Rate	h^{-1}
V_R	Reactor Volume	m^3
η_{CCUS}	Carbon Capture Efficiency	%
η_{ref}	Reference Efficiency Without Carbon Capture	%
ΔH	Molar heat of combustion	kJ/mol

1 Introduction

Given the fact that the energy sector is the largest contributor to greenhouse gas emissions and as the demand for electricity is rapidly growing; there is an increasing urgent need for new sources as well as developing existing ways of obtaining energy from renewables, while the integration of these renewable energy sources continues to increase. According to the World Energy Outlook 2018, global energy demand will grow by more than a quarter in 2040 in the New Policies Scenario. That is due to rising incomes and a global population growing by an estimated 1.7 billion people by that year. By 2040, low-carbon technologies, led by renewables, and natural gas will hopefully be able to meet more than 80% of the increase in global energy demand [1].

Energy and environment have been two of the most challenging and major issues of the world in recent years. The Global Energy Statistical Yearbook 2019 (fig. 1-1), states that the global energy consumption increased by 2.3% in 2018. This growth was the highest since 2010 [2]. The demand for all fuels has also increased, but growth was particularly strong in the case of gas (168 Mtoe, accounting for 43% of the global increase) and renewables (71 Mtoe, 18% of the global increase). In OECD (Organization for Economic Co-operation and Development) countries, energy demand increased by 82 Mtoe with gas demand growth as high as 70 Mtoe. In non-OECD countries, energy demand grew by 308 Mtoe with a gas demand of 98 Mtoe, coal 85 Mtoe and oil 47 Mtoe. On the other hand, the total CO₂ emissions from energy use grew by 2.0%, the fastest growth in seven years [3].

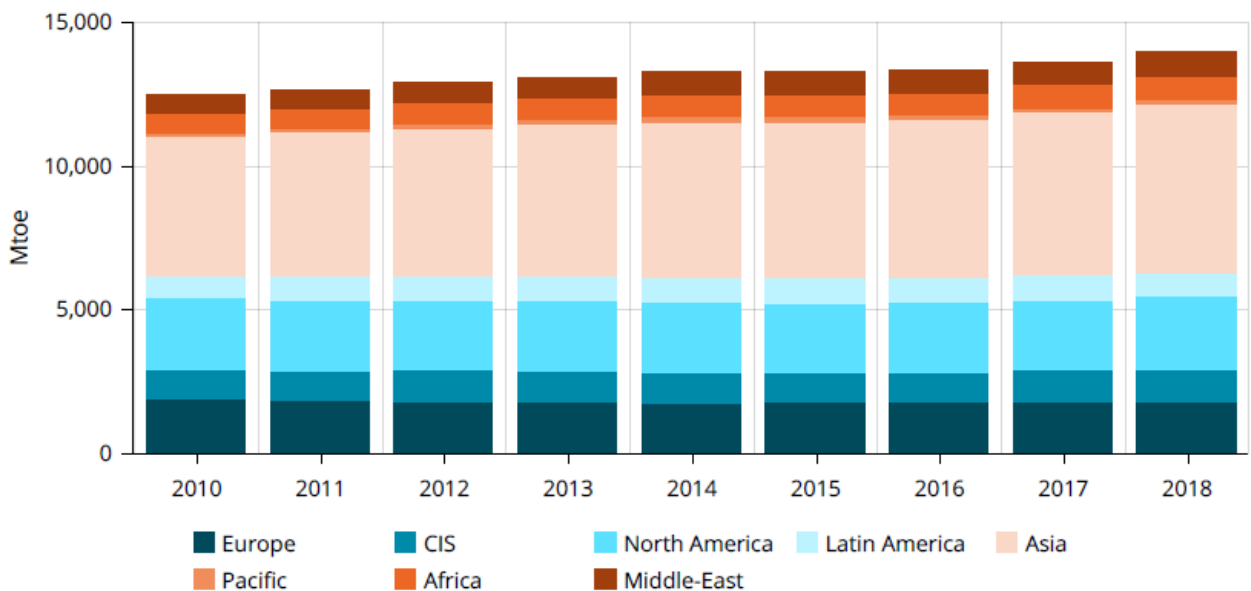


Fig. 1-1: Global energy consumption [Mtoe], 2010 – 2018 [2]

Over the past decades, efforts have been made in order to innovate and bring in new technologies to encounter environmental problems, energy shortages and reducing significant expenses of new power plants. Many researchers are working on implementing the most applicable technologies to fix some of these problems. Furthermore, storing energy waste from industrial,

commercial or domestic processes and minimizing the loss of energy have been vital in the world's battle with the increasing demand, amid continuous searches for new sources, growing ecological problems with greenhouse emissions and climate change. Energy storage's capability in reducing energy consumption, costs and that it may be used as a substitute for another energy source, all make it the certain future of research and development. Different storage technologies currently available are shown in fig. 1-2 [4].

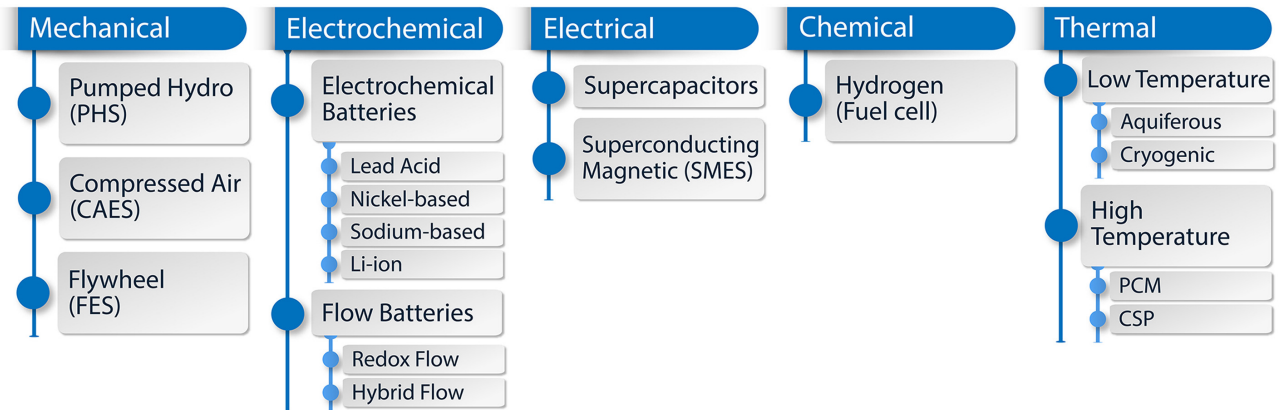


Fig. 1-2: Classification of energy storage technologies by the form of stored energy [5]

Since variable renewable energy sources (wind and solar) are weather dependent, meaning they have low dispatchability; their production levels often increase, causing power generation to exceed the demand, and so a proportion of the installed power must be reduced to maintain balance in the system. And thus, this excess energy is curtailed because it can't be utilized [6]. Power-to-gas (P2G) converts excess energy produced mainly by solar and wind power plants and stores it in the form of synthetic natural gas. This is done through a two-step process. H_2 is produced through the splitting of water by electrolysis. H_2 is fed CO_2 to produce methane through a process known as methanation. Methane (CH_4), the main component of synthetic natural gas (SNG) can be used for heating, transportation, long distance traffic, or electricity generation [7].

There are over 153 P2G projects currently in operation around the world, with several huge projects now being built. Data from multiple P2G projects and pilots from multiple countries are presented in [8]. Germany currently leads the way in production, with a total of nearly 40 MW followed by Denmark 20 MW [8]. Being the world's leader in this technology, Germany is targeting a 5 GW of P2G capacity by 2025 and 40 GW by 2050. [9].

The future of P2G looks to be promising, but that surely doesn't come without obstacles along the way. From high costs and low amounts of excess energy produced to importing gas and limited biomass potential, power-to-gas is yet to compete with other technologies currently used.

In this thesis, all the major parts of the power-to-gas system are thoroughly examined. Chapters 2, 3 and 4 present the main components of the methanation reaction: production of hydrogen through electrolysis, carbon capture and separation, Sabatier's reaction and types of methanation. A brief preview on OpenModelica is presented in the 5th chapter. While chapter 6 demonstrates the model that also includes electricity production from a photovoltaic power

plant. As well as presenting simulation results, analysis and an evaluation on the total operation and performance of the system. Finally, for purposes of comparison, a battery storage model with its respective efficiency are presented.

1.1 Power-to-Gas preview:

The following fig. 1-3 presents the power-to-gas chain. From electricity generation, to electrolysis, methanation and utilization of the product SNG.

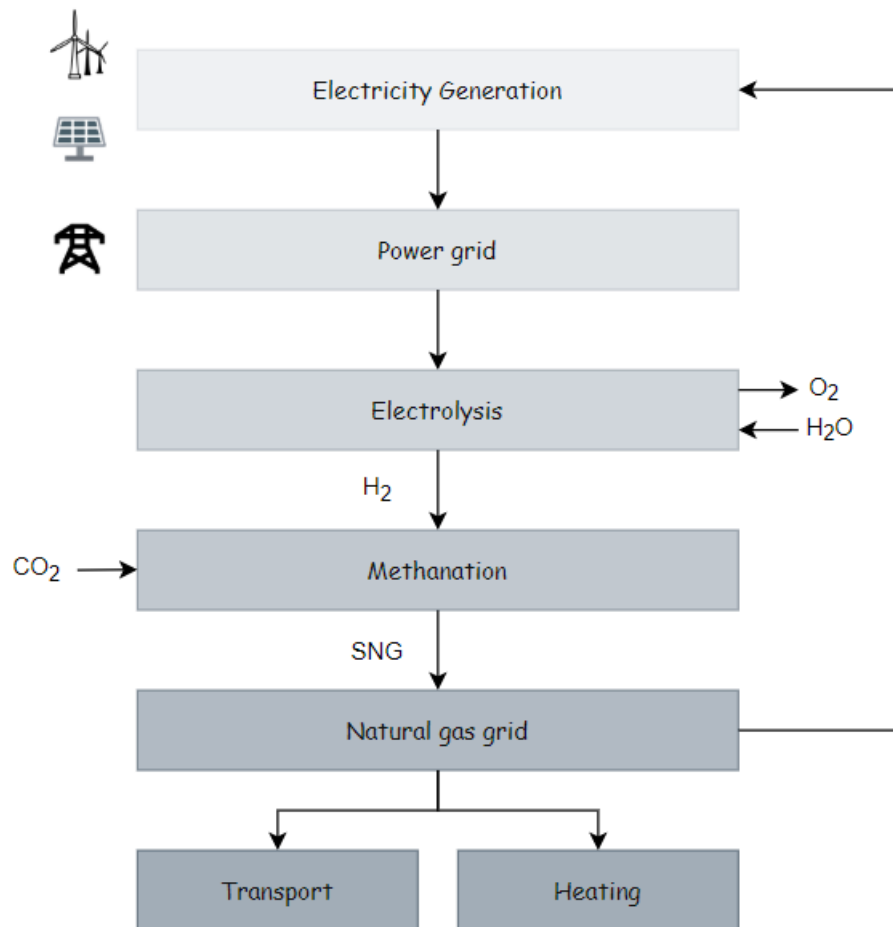


Fig. 1-3: Power-to-gas

2 Hydrogen supply

2.1 Properties

Tab. 2-1 lists hydrogen's basic physical and chemical properties. Hydrogen is the smallest element in the periodic table, having an atomic number of 1 and an average atomic weight of 1.0079 u, which make it the lightest element. Under normal conditions, it is nontoxic, nonmetallic, odorless, tasteless, colorless, and is highly combustible as H₂. Hydrogen is available in different forms, such as compressed gaseous hydrogen, liquid hydrogen, as well as solid and metallic forms [10].

Tab. 2-1: Basic properties of hydrogen [11]

Autoignition temperature	500	°C
Boiling point	-252.9	°C
Melting point	-259.14	°C
Density	0.08375	kg/m ³
Molar mass	2.02	g/mol
Specific heat at constant pressure, c_p	14.29	J/kg · K
Specific heat at constant volume, c_v	10.16	J/kg · K
Thermal conductivity	0.1825	W/m · K

2.2 Production

Hydrogen is a gaseous element occurring as its diatomic gas H₂. Since hydrogen does not naturally occur, it must be formed by the decomposition of other molecules. Approximately 95% of the hydrogen produced ($50 \cdot 10^6 \text{ t} \cdot \text{a}^{-1}$ around 50 million tonnes per annum) is produced by steam methane reforming and water-gas shift reaction. As for the remainder, it's produced through water electrolysis. Water electrolysis is considered to be a clean process, because other than hydrogen, oxygen is the byproduct in the output of this process [12].

Steam-methane reforming, a process in which high-temperature steam (700 °C – 1,000 °C) is used to produce hydrogen from a methane source, such as natural gas. First, in steam-methane reforming, methane reacts with steam under 3–25 bar pressure in the presence of a catalyst to produce hydrogen, carbon monoxide, and a relatively small amount of carbon dioxide. Hydrogen can be produced by steam-methane reforming using other fuels, such as ethanol, propane, or even gasoline. Second, in the water-gas shift reaction, the carbon monoxide and steam are reacted using a catalyst to produce carbon dioxide and more hydrogen. Carbon dioxide and other impurities are removed from the gas stream, leaving pure hydrogen [13].

Steam-methane reforming reaction:



Water-gas shift reaction:



In addition to combustion, hydrogen may also be exploited as an energy vector via catalytic recombination with oxygen. In contrast to the thermal energy produced in a combustion process, the catalytic reaction with oxygen produces electrical energy. This process is carried out using fuel cells to produce electrical energy, for example in fuel cell vehicles [10].

2.3 Water electrolysis

In the process of water electrolysis, water is decomposed by applying electric current to produce hydrogen and oxygen. This is done in 2 steps. At the positively charged anode the oxidation reaction takes place, while the reduction reaction occurs at the negatively charged cathode. The charge carrier can be OH^- , H^+ , or O_2^- [7]. There are 3 types of water electrolysis, Alkaline electrolysis (AEC) was the first technology to emerge. It is the most used alongside PEMEC, while SOEC is still in development [12].

The following is the overall reaction in a PEMEC:

Reduction reaction at cathode:



Oxidation reaction at anode:



Overall reaction:



2.3.1 Alkaline electrolysis

In this electrolyzer, an aqueous alkaline solution is used as an electrolyte, either KOH (Potassium Hydroxide) or NaOH (Sodium Hydroxide). The cathode and anode in fig. 2-1 are often manufactured from nickel and the separator between the anodic and cathodic chambers is a polymer which is permeable to hydroxide ions and water molecules. AEC is the oldest, simplest, and most durable electrolyzer technology. According to reports on AEC, such electrolyzers can be operated at 20% to 100% and overload up to 150%. This operation is compatible with P2G plants, that are connected to fluctuating sources of energy in solar and wind energy sources. Although being the most highly developed and the cheapest one, the alkaline technology has a disadvantage in the highly corrosive electrolytes such as potassium hydroxide. This means maintenance of the electrolyzers is necessary approximately every 7-12 years, while the expected lifetime of AEC electrolyzers is 20-30 years, which is relatively high compared to other technologies [7]. According to an international review of P2G plants, the average power of all installed alkaline electrolyzers is 98 kW [14].

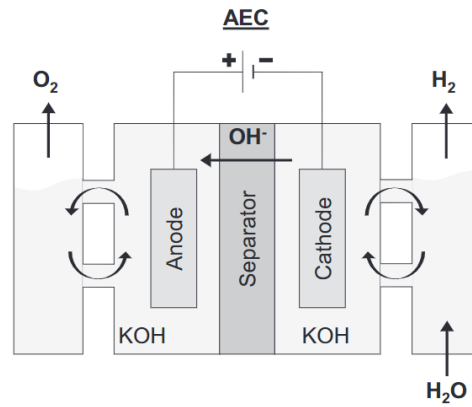


Fig. 2-1: Alkaline electrolysis [15]

2.3.2 Polymer electrolyte membrane electrolysis

In comparison with AEC, the PEMEC in fig. 2-2 is considered to be a new technology. First used in 1978, this technology uses a proton-conducting membrane of a sulfonated fluorinated polymer, such as Nafion. The thickness of the membrane depends on the conditions the electrolyzer operates on. Low-load operation require a thicker membrane to endure the high pressure and provide a suitable margin for material loss. The thinner the membrane is, the higher the efficiency of the process. This is due to the lower resistance with the the lower thickness. Electrocatalysts play an important role in speeding up the process of water oxidation. PEMEC's highly acidic nature, means that the choice of catalysts is limited to transitions metals which are stable under acidic conditions. Rhodium, ruthenium, platinum, iridium and their oxides are examples of transition catalysts. Currently platinum is being used on the cathode for proton reduction and iridium oxide at the anode for water oxidation [12]. According to international reports conducted on several power-to-gas pilots, the average nominal efficiency of PEMEC electrolyzers ranges between 52% to 79%. Furthermore, the average installed power of all PEMEC electrolyzers is 8.6 kW, which clearly shows that PEMEC are operated at lower power rates than alkaline electrolyzers [14].

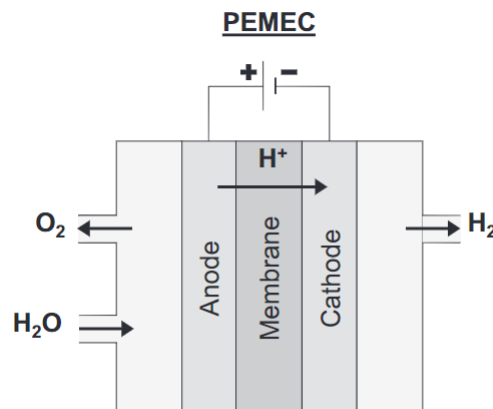


Fig. 2-2: Polymer electrolyte membrane electrolysis [15]

2.3.3 Solid oxide electrolysis

Solid oxide electrolysis operates at very high temperatures. This indicates that the electrolyzer is not fed with water, but rather with steam. The high temperatures decrease equilibrium cell voltage and consequently the electricity demand. This low demand is one of SOEC's most significant advantages. Fig. 2-3 below, illustrates solid oxide electrolysis' operation. In the solid oxide electrolysis process, high-pressure steam is reduced at the cathode to give hydrogen gas and oxygen anions. These anions move through the solid oxide electrolyte and are oxidized to produce oxygen gas. The electrons produced travel around the external circuit and supply the electrons for the water reduction. The product gases diffuse through the porous electrodes [12].

SOEC certainly encounters problems caused by high temperatures. For example, fast material degradation and limited long term stability. Furthermore, high temperatures mean that the electrolyzer's product is a mix of hydrogen and steam, increasing the capital costs [7].

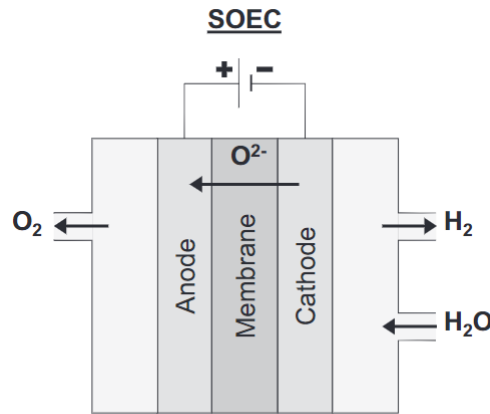


Fig. 2-3: Solid oxide electrolysis [15]

Tab. 2-2: Comparison of parameters of AEC, PEMEC, and SOEC [7]

	AEC	PEMEC	SOEC
State of development	Commercial	Commercial	Laboratory
H₂ production in m³	<760	Up to 450	-
Electrolyte	Alkaline solution	Solid polymer membrane (Nafion)	ZrO ₂ ceramic doped with Y ₂ O ₃
Cell temperature in °C	40-90 °C	20-100 °C	800-1000 °C
Cell voltage in V	1.8-2.4 V	1.8-2.2 V	-
Disadvantages	Low current density Maintenance costs Highly corrosive system	Expensive Fast degradation	Limited long term stability of the cells Not suitable for fluctuating systems Expensive
Advantages	Available for large plant sizes Cheap Relatively long lifetime	No corrosive substances High power densities High pressure >100 bar	High efficiency Possible integration of waste heat

Tab. 2-2 compares all three electrolysis technologies. In addition to the advantages and disadvantages of each electrolyzer, it presents parameters that affect electrolyzer's operation, such as the type of electrolyte, cell temperature and cell voltage.

2.4 Hydrogen transport

According to [16] hydrogen can be transported to facilities in several ways. Compressed gas cylinder, cryogenic liquid and pipelines are amongst them.

2.4.1 Compressed gas cylinder

Gaseous hydrogen can be transported in small to medium quantities in compressed gas containers by lorry. For transporting larger volumes, several pressurized gas cylinders are attached together to form CGH₂ tube trailers. The tubes are usually made of steel and have a high net weight. This can lead to mass-related transport restrictions. Hydrogen's low density also influences its transport. At STP (101.325 kPa and 273.15 K), hydrogen has a density of 0.0899 kg/m³) [16].

2.4.2 Cryogenic liquid

Hydrogen can also be transported in liquid form in lorries or other means of transport. Because the density of liquid hydrogen is higher than that of gaseous hydrogen, LH₂ tubes can carry more hydrogen. Hydrogen transported in its liquefied state is more cost-effective since a liquid hydrogen tank can hold more hydrogen than a pressurized one. In liquid transport the hydrogen is loaded into insulated cryogenic tanks. LH₂ trailers can be as long as 4,000 km [16].

2.4.3 Pipelines

A pipeline network is a very effective method for largescale hydrogen transportation. By 2016, there were more than 4,500 km of hydrogen pipelines worldwide [16].

3 Carbon Dioxide Sources

After a period of low rate emissions due to weak economic growth, CO₂ emissions grew by 2.1% 2017 and 1.9% by 2018. Europe and Latin America haven't been contributing to these emissions. As for China, emissions have risen to reach 3.1%, in India 4.2%, Russia 2.9% and in the US 3.1%. Emissions in Europe have declined by 2.1%, with policies to reduce energy demand have been made by European countries led by Germany. Japan's implementation of solar energy and higher nuclear generation, have led to five years of continuous decline in emissions. According to the Paris agreement held in 2016, although CO₂ intensity has relatively decreased on a average between 2000 and 2017 by a 1.7% year rate, intensity levels reduction is still not enough. According to British Petroleum's Statistical Review 2019, the worlds CO₂ emissions has increased from 33242.5 MtCO₂ to 33890.8 MtCO₂ in 2018, with China contributing to 27.8% [2]. British Petroleum's Energy Outlook 2019 states that by 2040, the global power sector will be responsible for 40% of the CO₂ emissions, more than transport and industry [17].

Amid international fears of increasing climate change and global warming, limiting CO₂ emissions is a priority in future scenarios concerning energy sources, demand, storage, and transition. CO₂ emissions' prevention can be achieved by utilizing, storing and recycling carbon dioxide produced during fuel combustion in power plants [18].

CO₂ sources for power-to-gas applications

The CO₂ required can be a produced from either fossil fuels or renewable sources. Fossils are considered to be produced by power plants or industrial processes. As for the CO₂ produced from renewable sources, we consider biogas, biomass and other fermentation processes that use anaerobic digestion. Furthermore, CO₂ can be absorbed from the atmosphere [18]. The following fig. 3-1 demonstrates different CO₂ sources with their relative concentrations.

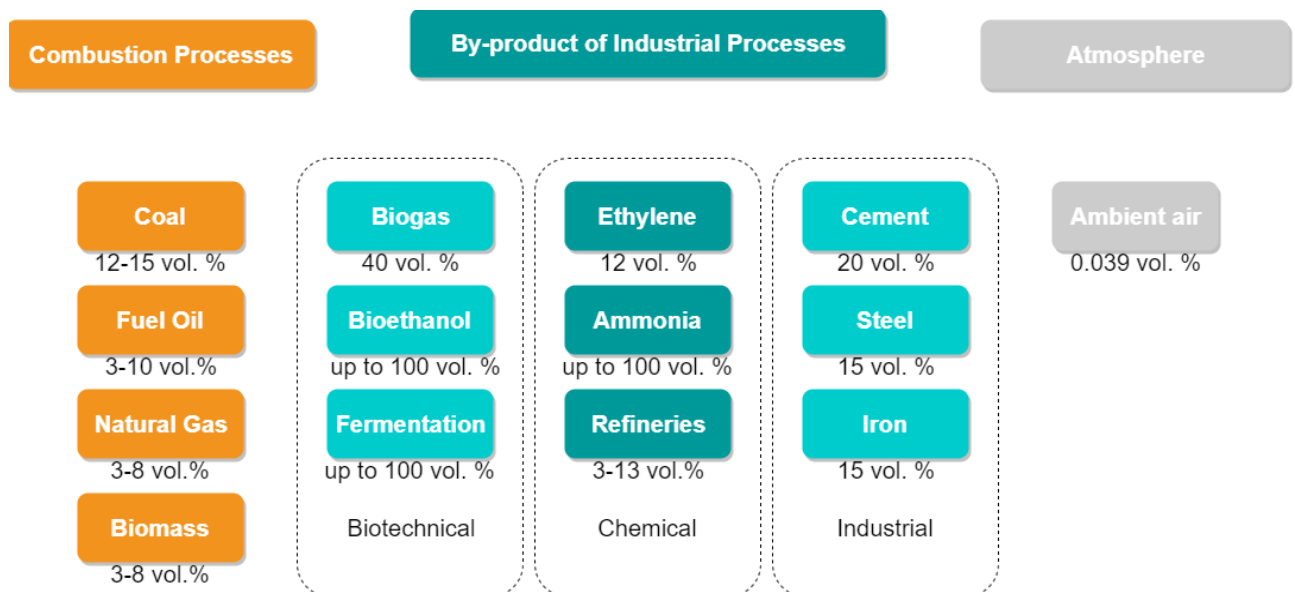


Fig. 3-1: Different CO₂ sources with their relevant concentrations [18]

Most CO₂ sources produce CO₂ at relatively low concentrations (up to 15 vol.%), while there are some exceptions with some sources producing CO₂ at very high concentrations. The purity of CO₂ in the exhaust gas influences the efficiency of subsequent operations in the process. Therefore CO₂ separation technologies are further used to purify and consequently increase efficiencies [18].

3.1 CO₂ from combustion processes in power plants.

During the combustion of fossil fuels such as coal, natural gas, and fuel oil, plus biomass combustion¹, the flue gas produced contains a relatively small percentage of CO₂ in it, therefore CO₂ capture and consequently its separation is required.

One method has emerged in recent years, and that is Carbon Capture, Utilization and Storage (CCUS).

3.1.1 CO₂ capture

There exists 3 methods of CO₂ capture in combustion processes [18].

- post-combustion (CO₂ capture from flue gas)
- pre-combustion (CO₂ capture before combustion)
- oxyfuel processes

Post-combustion capture

Post-combustion capture refers to capturing carbon dioxide from the flue gas exhausted after burning the fuel. Post-combustion processes capture CO₂ at 85-90% efficiency. In fig. 3-2 post-combustion carbon capture in a combustion plant is shown. [19].

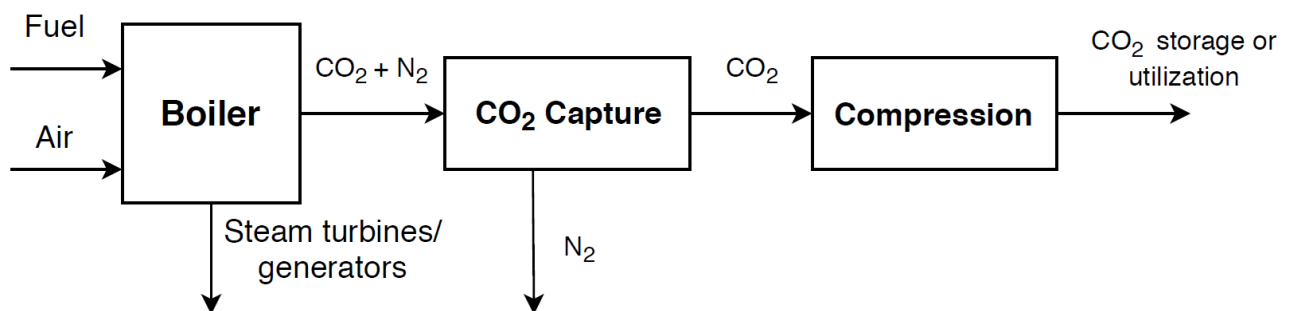


Fig. 3-2: Post-combustion capture [21]

Pre-combustion capture

In integrated gasification combined cycle power plants (IGCC), solid fuel such as coal is converted into gaseous fuel (syngas) by applying heat under pressure in the presence of steam and oxygen. Further the syngas reacts in a water-gas-shift reaction to produce hydrogen and

¹Considered as carbon-neutral, meaning CO₂ capture would have a decrease on the power plant's efficiency.

carbon dioxide (CO_2). Carbon is captured from the syngas before it is further combusted in the gas turbine to produce electricity. In the pre-combustion method efficiencies reach 95%. Fig. 3-3 shows pre-combustion carbon capture in a combustion plant [20].

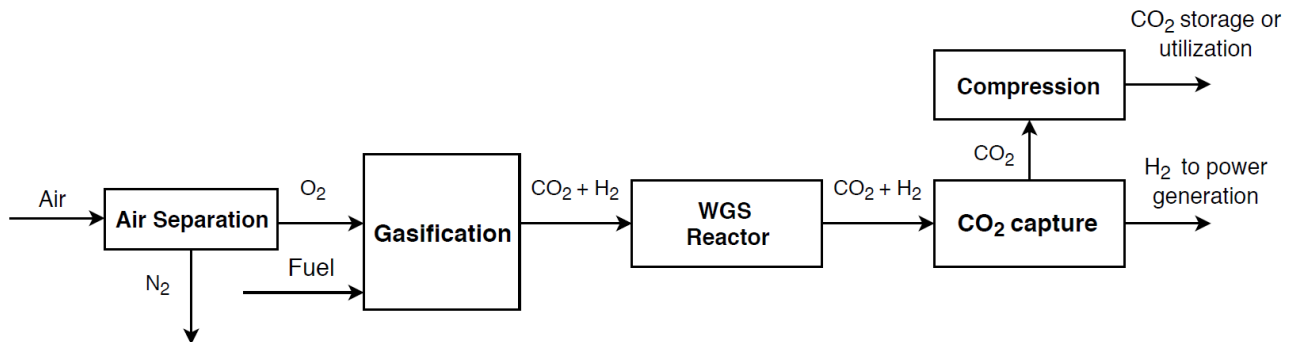


Fig. 3-3: Pre-combustion capture [21]

Oxyfuel

In order to avoid nitrogen in the exhaust gas, fuel is burned with pure oxygen.. The recycled flue gas is inputted back to the boiler to prevent the combustion temperature from becoming too high. This oxygen-rich, nitrogen-free exhaust gas results in final flue-gases consisting mainly of CO_2 and H_2O , which can be removed by cooling and compression. Oxyfuel efficiencies are approximately 90%. In fig. 3-4 we can see oxyfuel carbon capture in a combustion plant. And its worth mentioning, that in the oxyfuel process, further separation is not required because fuel is burnt with pure oxygen, in the absence of nitrogen [18].

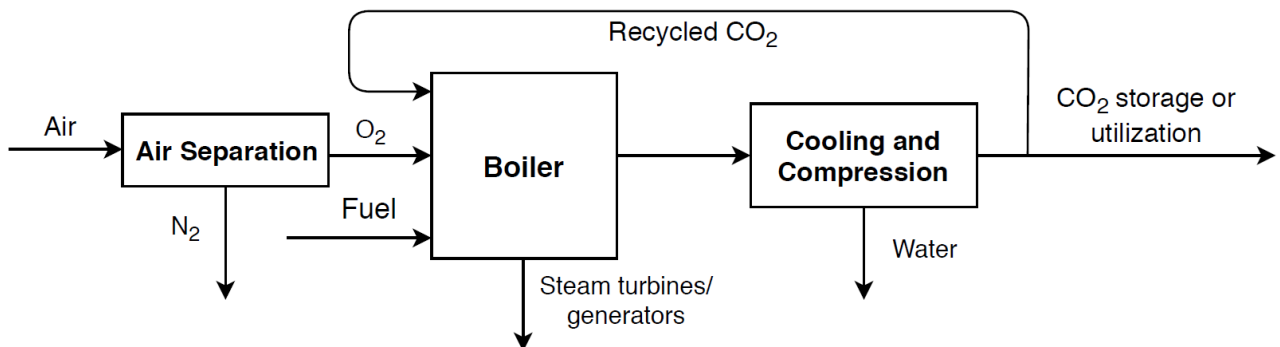


Fig. 3-4: Oxyfuel capture [21]

3.1.2 CO_2 separation technologies

As stated before, after CO_2 capturing, its separation from other gases is required. Absorption, adsorption, cryogenics, membranes, and microbial/algal systems, are examples of separation technologies used.

Absorption

This technology works basically by absorbing CO_2 into a liquid. The absorbent loaded with CO_2 is transported and CO_2 is released by heating or depressurization. The regenerated absorbent is then sent back to the absorption column. Absorbents can be chemical or physical. Chemical ones are for example amines, aqua ammonia and sodium carbonate. Alcohols, polyethyleneglycol and other oxygenated compounds are used as physical absorbents [22].

Adsorption

Adsorption uses a solid sorbent to bind CO_2 . The gas mixture is compressed and injected into a vessel, where CO_2 is adsorbed on the surface of the adsorbent. Then CO_2 is released by depressurization and heating. Examples of adsorbents are activated carbons, zeolites and amine functionalized adsorbents [22].

Cryogenics

Cryogenic distillation splits CO_2 from a gas mixture by condensation. The gas mixture is compressed and cooled down in the heat exchanger. The cooled pressurized fluid mixture is then fed into distillation [22].

Membranes

Different flows are used in a membrane: the feed (gas mixture), retentate (CO_2 -poor gas) and the permeate (CO_2 -rich gas). The feed enters, and the permeate passes through the membrane and CO_2 -rich gas exits the membrane [22].

Fig. 3-5 shows the different separation technologies.

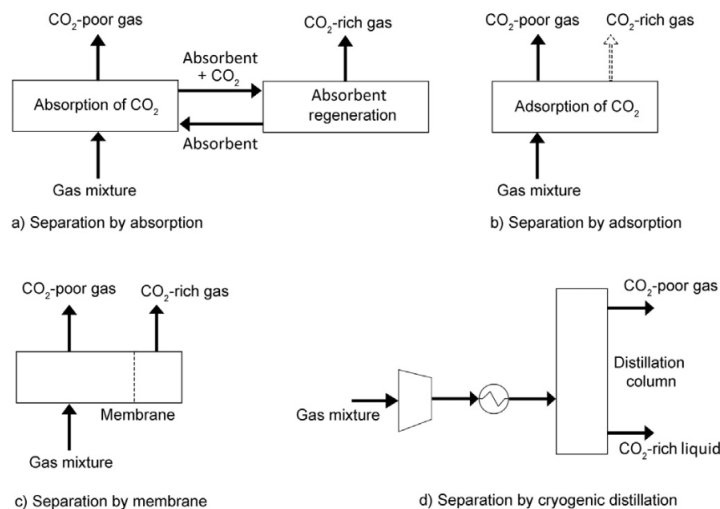


Fig. 3-5: CO_2 separation technologies [22]

3.1.3 Energy penalty in CCUS

A CCUS plant requires power to be integrated and to operate equipment. The addition of CCUS leads to the decrease in net efficiency. The energy penalty is defined as the reduction in the net electrical energy caused by the integration of the CCUS plant. Energy penalty is also defined as the the increase in the required fuel to maintain power output after the addition of CCUS. In other words, the net power will decrease, due to the load put the implementation of CCUS. Energy penalty is expressed by eq. 3.1 and in fig. 3-6 [23]:

$$EnergyPenalty = 1 - \frac{\eta_{CCUS}}{\eta_{ref}} \quad [-] \quad (3.1)$$

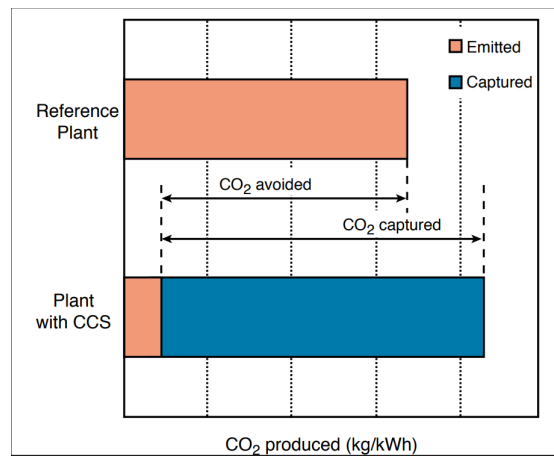


Fig. 3-6: CO_2 emission intensity with and without carbon capture [24]

3.2 CO_2 from industrial processes

Biogenic CO_2 sources include the combustion of biogas collected from biological decomposition of waste in landfills, wastewater treatment, or manure management processes. In addition to the combustion of the biological fraction of municipal solid waste or biosolids, CO_2 is also derived from combustion of biological material, including forest-derived and agriculture-derived feedstocks [25].

As mentioned in fig. 3-1, CO_2 can be a by-product of several industrial processes. Biogas' main component are CH_4 (50 - 70%) and CO_2 (30 - 50%) with others considered as trace components. After biogas production from anaerobic digestion, its separated to obtain biomehtane for further injection into the gas grid [7]. Further CO_2 is produced as result of chemical industrial processes such as in ammonia production plants. It can also be captured in refineries such as steam cracking or ethylene production. In addition to that, CO_2 is also produced in large amounts in iron and steel production. The ironmaking industry produces CO_2 in high concentrations (25 - 30 vol.%) and capture efficiencies up to 90%. Finally, the productions of mineral products such as cement, clinker and lime also have high CO_2 emissions [18].

3.3 CO₂ captured from the atmosphere

Apart from CO₂ capturing from combustion and industrial processes, it can also be captured from the atmosphere. This process is relatively complex due to the low concentration of CO₂ in the atmosphere [18].

3.4 CO₂ transport

The CO₂ captured is transported to the methanation facility. It can be transported as compressed or liquefied. It can be transported in large amounts by truck or via pipelines over hundreds of kilometers [7]. Pipelines can transport CO₂ in three states: solid, liquid and gaseous, but they commonly transport carbon dioxide in its gaseous state [26].

4 Methanation

Synthetic natural gas (SNG) or substitute natural gas is an artificially produced version of natural gas. The carbon-containing mass can be gasified; the resulting syngas can then be converted to methane, the major component of natural gas [27].

The SNG produced from P2G plants must have similar properties to natural gas. Natural gas has more than 80% of methane in it. Further, SNG's lack of higher hydrocarbons may result in low calorific value² compared to that of natural gas [27].

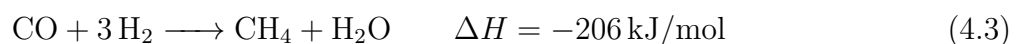
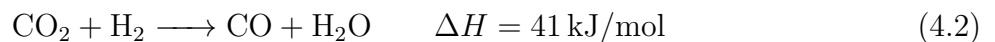
In a chemical reaction known as methanation, carbon monoxide CO or carbon dioxide CO₂ is converted to methane through hydrogenation. This methanation reaction works according to what is known as the Sabatier reaction proposed in 1902 by Paul Sabatier. Methanation has gained a lot of industrial importance in power-to-gas.

4.1 Thermodynamics

Methanation is an exothermic reaction, it is thermodynamically favored at relatively low temperatures and high pressures [28]. This is presented in the following reaction:



One mechanism of methanation is the linear combination of the endothermic reversed water-gas shift reaction (4.2) and an exothermic CO methanation (4.3) [28]



4.2 Effects of pressure, temperature and H₂ : CO₂ ratios

High carbon conversion is a very crucial parameter for the methanation plant's performance, economics and efficiency. In an experiment conducted by [29] on carbon dioxide methanation reaction in a tubular, fixed-bed reactor, CO₂ conversion was evaluated. The catalyst used was nickel. The reactor was operated at different temperatures and H₂ : CO₂ ratios to determine optimum operating conditions. Results showed high conversion rates with H₂ : CO₂ ratio of 6:1 to have the highest conversion of about 80% and maximum conversion to be between 300 °C and 325 °C. Increasing the temperature above 450 °C results in more CO by-product, due to reversed water gas shift reaction. But the stoichiometric ratio for H₂/CO₂ 4:1 results in the highest equilibrium concentration of CH₄, which makes it more recommended. The unreacted hydrogen in higher ratios such as 6:1 or 5:1, dilutes the concentration on the mixture and lowers CH₄ concentrations.

The following fig. 4-1, presents the effects of pressure and temperature with H₂ : CO₂ = 4 on the reaction. Pressures of 30 atm (3040 kPa) and above, have led to the best results for

²The calorific value of a fuel is the amount of heat produced by the complete combustion of a specified quantity of it.

CH_4 yield, CH_4 selectivity and CO_2 conversion rates. CO_2 conversion rates, and consequently CH_4 (fig. 4-2) yield are highest at low temperatures between 200 °C and 450 °C [30].

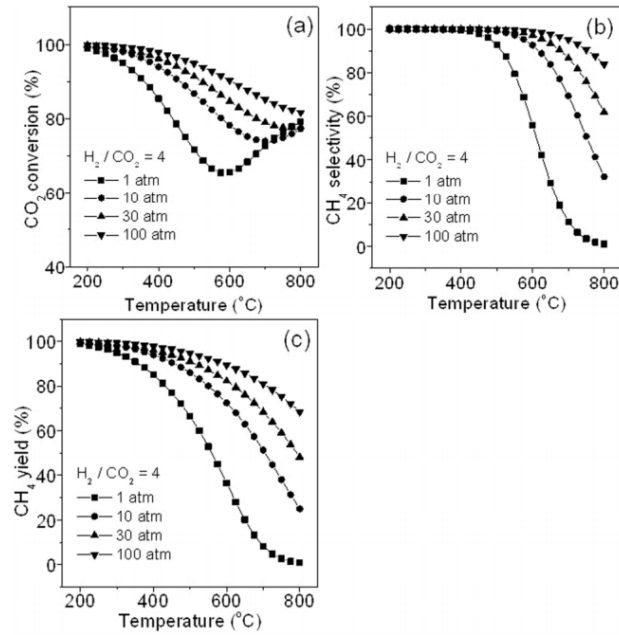


Fig. 4-1: Effects of pressure and temperature with $\text{H}_2/\text{CO}_2 = 4$ on CO_2 methanation: (a) CO_2 conversion, (b) CH_4 selectivity, and (c) CH_4 yield [30]

In fig. 4-2 the percentage of methane in the SNG produced at different rates of CO_2 conversion is shown. It shows that CO_2 conversion rates required reach as high as 97% to produce $>90\%$ CH_4 [7]. In conclusion, low temperature, high pressure, and the right $\text{H}_2 : \text{CO}_2$ ratio results in optimum CO_2 methanation.

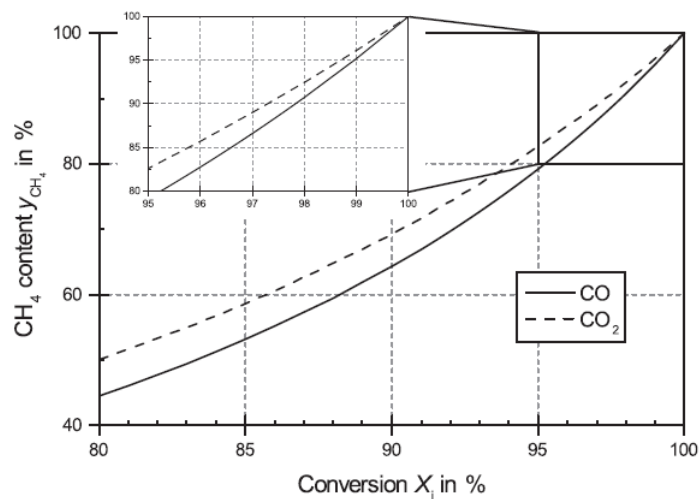


Fig. 4-2: CH_4 content at different CO_2 conversion rates [7]

4.3 H₂–CO₂ separation and recycle

One of the most important demands in the composition of the produced methane is achieving a product molar composition of less than 2%. Thus the unconverted CO₂ must be separated and recycled. In a techno-economic study [31] conducted on P2G strategies, 3 reactor stages were used. The first reactor has the highest concentration and pressure, and 80% CO₂ conversion. The second reactor had a lower pressure and lower conversion rates of 70% while the third one had lower pressure and 60% conversion. Further, three separation and recycling stages were analyzed. First, a 40% bulk recycle, next is 90% CO₂ separation and recycle and lastly a 90% H₂ separation and recycle. The produced SNG had 92.7% CH₄, 6.3% H₂ and 1.0% CO₂. This bulk gas recycle is meant to increase the reaction conversion rates. This separation is simply done in a diverter. CO₂ removal is necessary in controlling the amount of CO₂ in the product. Fig. 4-3 shows the molar gas composition at each stage of the reactors and recycling.

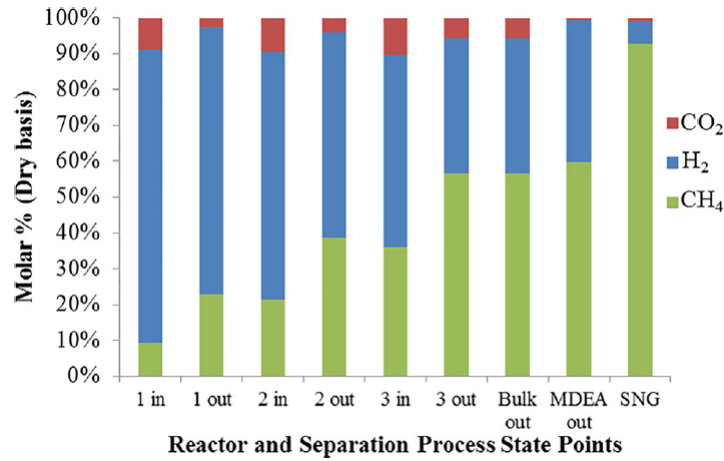


Fig. 4-3: Molar gas composition at various stages [31]

Methanation can be achieved in biological or catalytic methanation reactors.

Before getting into details on reactor performance later in this chapter, it's worth mentioning *GHSV* (Gas Hourly Space Velocity) which is an important parameter in studying reactor performance and comparing biological and catalytic methanation [7].

$$GHSV = \frac{F_{V,G,in}}{V_R} \quad [\text{h}^{-1}] \quad (4.4)$$

4.4 Catalytic methanation

Catalytic reactors are operated at temperatures ranging between 200 °C and 550 °C and pressures ranging from 1 to 100 bar. Catalytic methanation reactors use catalysts such as Nickel (Ni), Ruthenium (Ru), Rhodium (Rh) and Cobalt (Co), but mainly Ni is considered the optimum catalyst, due to its relatively high activity, good CH₄ selectivity² and low raw

²The ability to direct a reaction to produce a certain product

material price. Maintaining a good temperature control, meaning proper heat removal, in order to prevent catalyst sintering or thermodynamic limitation is the main issue facing methanation reactors [7].

4.4.1 Adiabatic fixed-bed reactors

In fixed-bed reactors, the reaction takes place in the form of heterogeneously catalyzed gas reaction on the surface of catalysts, that is the so called fixed-bed in the reactor (fig. 4-4). The catalyst is present in a form of uniform fixed-bed surrounded by an outer insulating jacket [32]. The usual operation in fixed-bed reactors relies on a series of 2-5 adiabatic reactors, with inter-cooling and gas circulation like in multi-tubular reactors. The catalyst in such reactors, must be able to endure temperatures between 250 °C and 700 °C . The main problem facing fixed-bed reactors is possible cracking or sintering. Such reactors operate at a relatively fast rate of GHSV = 2000 - 5000 h⁻¹ [7].

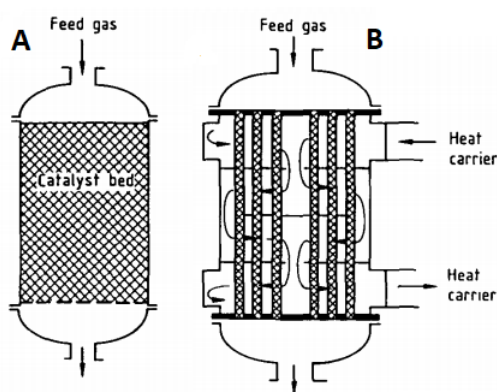


Fig. 4-4: Catalytic fixed-bed reactors A) Adiabatic fixed-bed reactor; B) Multi-tubular fixed-bed reactor [32]

4.4.2 Fluidized-bed reactors

A large amount of heat is generated in methanation reactors during the production of SNG. The main goal in the design of catalytic reactors is to achieve efficient removal of that heat in order to minimize the deactivation of the catalyst due to thermal stress and to prevent reducing the yield of methane due to the approach of the chemical equilibrium. And that allows for using one single reactor with a simpler design. In fluidized-bed reactors (fig. 4-5), the mixing of fluidized solids allows for an isothermal one-step operation facilitating control. Furthermore, the movement of the catalyst particles through the bed and the possibility of combining the water gas shift and methanation reaction in one apparatus enables a long catalyst stability due to internal regeneration of the catalyst. The disadvantages of fluidized-bed reactors are the need for an erosion resistant catalyst and the difficulties in scale-up [7, 33].

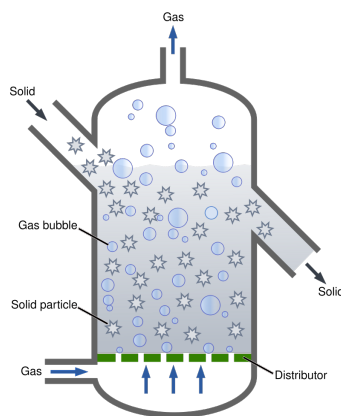


Fig. 4-5: Fluidized-bed reactor [34]

4.4.3 Three-phase reactors

Catalyst deactivation is a major problem faced in both fixed-bed and fluidized-bed reactors. With sintering problems in fixed-bed reactors and attrition in fluidized-bed reactors causing the mentioned deactivation to occur. To tackle such problems, three-phase reactors (fig. 4-6) are considered to be a better option for methanation, where a solid catalyst (size $<100 \mu\text{m}$) is present in a temperature stable inert liquid. The presence of the liquid phase with high heat efficiency allows efficient temperature control: the reaction heat can be removed completely and the reactor can operate almost isothermally, resulting in a simple process design. However, a major drawback in three-phase methanation reactors is gas-liquid mass transfer resistances. GHSV of such reactors is around $500 - 1000 \text{ h}^{-1}$ [7].

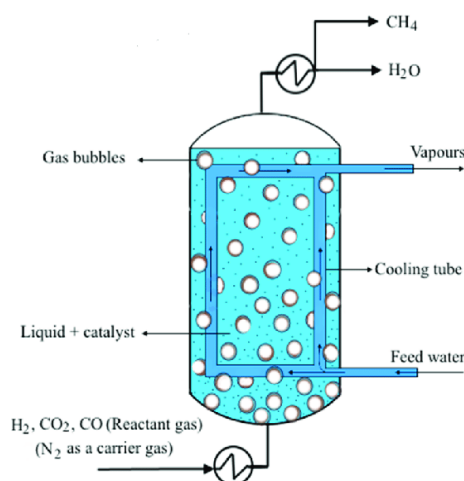


Fig. 4-6: Three-phase reactor [34]

4.4.4 Structured micro-reactors

With temperature hot spots and high pressure drops in adiabatic fix-bed reactors, a new technology has emerged in recent years to solve such problems and that is of structured reactors, such as monolith, micro-channel and milli-fixed bed reactors. Due to the internal metallic

structure, heat conduction in the metal gives structured micro-reactors an advantage over other reactors with better radial heat transport in the conductive metal. Structured micro-reactors are very compact reactors. They have high surface-to-volume ratios. Disadvantages accompanying micro-reactors are catalyst deposition on the metal as well as replacing deactivated catalysts (the whole reactor would need a new catalyst once the old one is deactivated) [7]. Fig. 4-7 shows three kinds of structured micro-reactors with their respective internal structures.

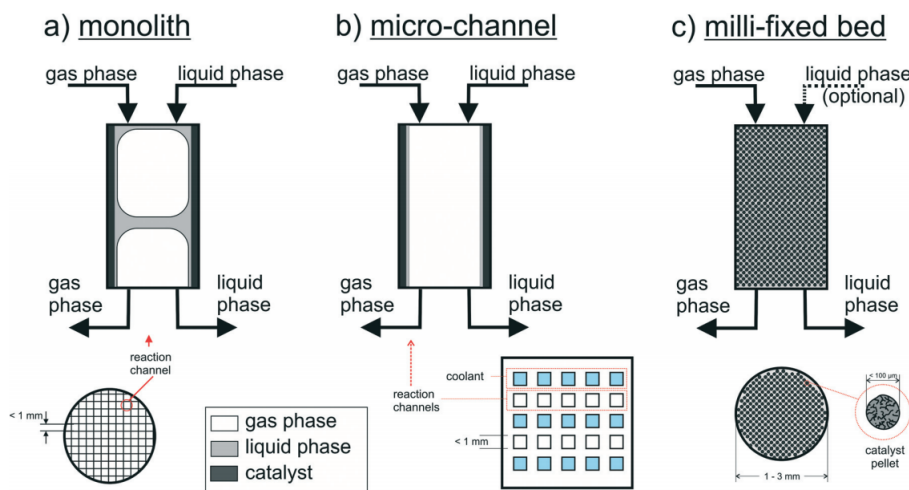


Fig. 4-7: Structured micro-reactors [35]

4.4.5 Catalyst and reactor requirements

A catalyst is a chemical substance which alters the rate of a reaction while not being consumed and doesn't undergo any permanent chemical change during the reaction. In methanation reactions, and as mentioned before, Nickel (Ni) is mostly used. The methanation reactor can be operated under steady-state or dynamic-state. In steady-state, a constant flow of H_2 is required to ensure steady operation, But this affects the facility economically, as this augments the facility. Dynamic-state operation means there are certain requirements that catalyst and reactor should have to sustain the operations. The catalyst should also be able to withstand high temperatures and long operation time, to avoid its deactivation [7].

As for the reactor, certain parameters influence its operation, namely reactor pressure, temperature, gas velocity (GHSV), catalyst concentration, and reactant partial pressures. In other words, it should be able to work with temperature and pressure variations and fluctuating feed streams. Reports on experiments show that temperature increase is inevitable in adiabatic reactors after a strong gas feed. Isothermal reactors (fluidized fixed-bed reactors) showed a better temperature regulation under dynamic operation [7]. And according to a study reported by [36], three-phase methanation reactors showed relatively constant temperatures while increasing gas flow from 25% to 100%. In addition to the mentioned above, rapid start-ups and shut-downs are required in case of a needed total shutdown [7].

4.5 Biological methanation

Biological methanation is another option for CO₂ methanation to produce SNG. In this case, methanogenic microorganisms are used as the so-called biocatalysts. In biological methanation, methane is produced by hydrogenotrophic methanogenesis from CO₂ and H₂. Biological methanation works at temperatures between 20 °C and 70 °C and at ambient pressure. Efficiencies of biological methanation are influenced by several parameters, such as the type of microorganisms, cell concentration, reactor type, pH, pressure and temperature [7].

Methanation Formation Rate

$$MFR = \frac{F_{V,CH_4}}{V_R} \quad [h^{-1}] \quad (4.5)$$

Methanation reaction takes place in an aqueous solution. This means the existence of gas-liquid mass transfer resistance. The solubility of hydrogen is an important step to make gaseous hydrogen available for microorganisms. Its solubility in water is relatively low compared to that of CO₂ ($H_{H_2,H_2O} = 1408$ bar l/mol and $H_{CO_2,H_2O} = 36$ bar l/mol) according to [7]. The hydrogen to liquid transfer is therefore an obstacle in this process.

The effectiveness of the reaction can be increased by improving the mass transfer or increasing the solubility, thus increasing hydrogen's transfer to the liquid. As a result, MFR , presented in eq. 4.5, increases due to improved supply of H₂ consequently the production of CH₄ [7].

Biological Methanation is possible in a separate reactor or in situ digester

4.5.1 Biological methanation in a separate reactor

In this type of biological methanation, pure gases are converted to SNG in a separate reactor by methanogen cultures. In the case of biogas, this increases the calorific value. Because the process takes place in a separate reactor, the hydrogenotrophic methanogens' conditions can be adjusted. There are various types of reactors used in order to improve MFR: CSTR, fixed-bed, trickled-bed reactors are among those reactors [7]. Fig. 4-8 shows a block diagram of biological methanation in a separate reactor.

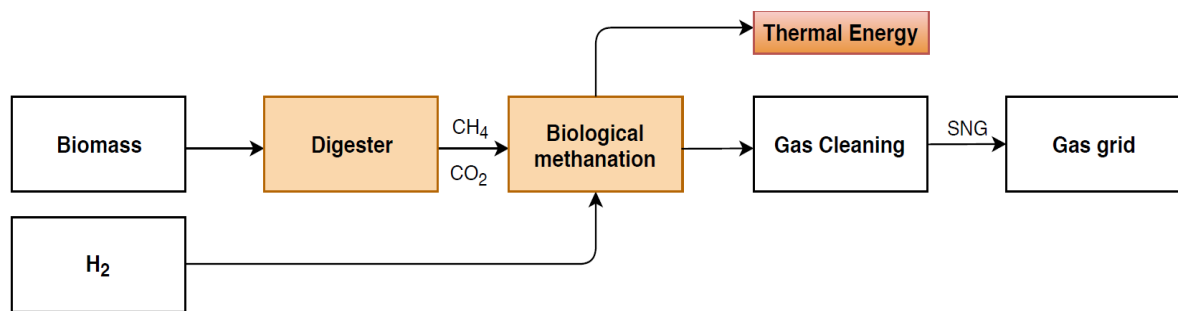


Fig. 4-8: Biological methanation in a separate reactor [7]

In [7], a range of reactor performances is reported. It shows that high MFRs (21.3 and 28.7h⁻¹) were achieved using CSTRs operated at GHSV of 120 and 300 h⁻¹, respectively. But

the results show a low content of methane in the product gas (60% and 13.4%). Another experiment reported a methane content of 85% in the reactor outlet by reducing the GHSV by a factor of 4. Consequently MFR also decreased by nearly 75%. However, a methane concentration of 98% in the product gas was obtained by using a trickle-bed reactor at a relatively low GHSV = 0.3 h^{-1} . Further studies reported by [7] show a MFR of 4.6 h^{-1} and a pure product yield of 34% in fixed-bed reactors. The MFRs reported in trickle-bed or fixed-bed reactors are relatively lower than in CSTRs. But on the other hand a stirrer isn't necessary and thus the energy consumption is lower.

4.5.2 In situ biological methanation

In this biological methanation, a part of the CO_2 produced from the biogas in the digester is fed hydrogen to produce a high content methane biogas. MFR in this case ($<0.1 \text{ h}^{-1}$) is limited by the CO_2 production rate. Fig. 4-9 shows a block diagram of biological methanation in situ reactor.

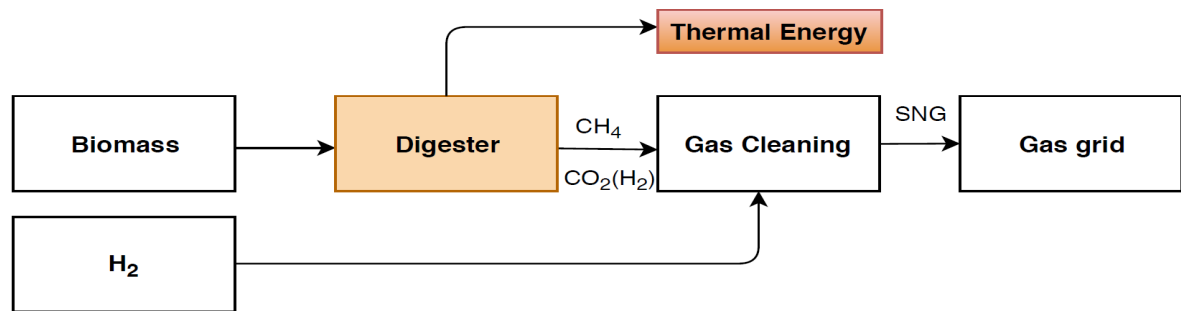


Fig. 4-9: In situ biological methanation [7]

4.6 Methanation parameters

This section deals with various aspects of methanation including different types of reactors.

4.6.1 Tolerance of impurities

Impurities in methanation mainly occur in the form of hydrogen sulfide in the feed gas. According to reports mentioned in [7], components such as sulfur and oxygen had no effect on biological methanation. On the contrary, sulfur and sulfur-containing components are considered to be poisonous to the catalyst such as nickel. The reports state a sulfur content of $\ll 1$ ppm must be obtained in the gas feed. Further problems are associated with H_2 composition. In the SNG 17% of H_2 has been deemed to be acceptable [7].

4.6.2 Load change

Different parts of the reactor react very fast to load changes. Fixed-bed reactors are the most sensitive. Reports show that load changes affect the catalyst bed, causing fluctuating temperatures (cooling down of the reaction) [7].

4.6.3 Shutdown

Reports on load change from 100% to 0% show no negative consequences in biological methanation. However, in catalytic methanation the reactor must be flushed with hydrogen or inert gas before complete shutdown [7].

4.6.4 Wobbe index

The Wobbe index in eq. 4.6 is a very important measure in the combustion of gases, it helps indicates the burner's ability to proceed with the combustion of the used fuel. The Wobbe index is a measure of the mixing of fuel gases and their relative ability to deliver energy [31].

$$I_b = \frac{HHV_{SNG}}{\sqrt{\frac{\rho_{SNG}}{\rho_{air}}}} \quad [\text{MJ}/\text{Nm}^3] \quad (4.6)$$

where,

- I_b Wobbe index $[\text{MJ}/\text{Nm}^3]$
- HHV_{SNG} Higher heating value $[\text{MJ}/\text{Nm}^3]$,
- ρ_{SNG} Density of the produced SNG $[\text{kg}/\text{m}^3]$
- ρ_{air} Density of air $[\text{kg}/\text{m}^3]$, $\rho_{air} = 1.205 \text{ kg}/\text{m}^3$.

SNG has a lower volumetric energy density based on the Wobbe index. While natural gas has a higher volumetric density, because it contains 10% ethane (C_2H_6), 5% propane (C_3H_8), 2% butane (C_4H_{10}), and 0.5% pentane (C_5H_{12}), all which makes natural gas heavier than SNG [31].

To increase plant's efficiency, heat produced as a result of the highly exothermic reaction must be removed. For example, the waste heat can be utilized to heat a biogas digester [7].

5 Openmodelica

OpenModelica is a free open-source environment used for modeling and simulating complex systems. It can be installed on Linux, MS Windows or Mac OS operating systems. It is based on the Modelica modelling language. OpenModelica Connection Editor (OME) serves as an open-source graphical user interface. OME also has libraries that contain prepped components and examples. There is a variety of libraries such as Photovoltaics, Power Systems or Electrical Energy Storage. The main library is Modelica, it consists of sub-libraries like math, electrical, magnetic and more. Fig. 5-1 presents the modelling perspective of OME [37].

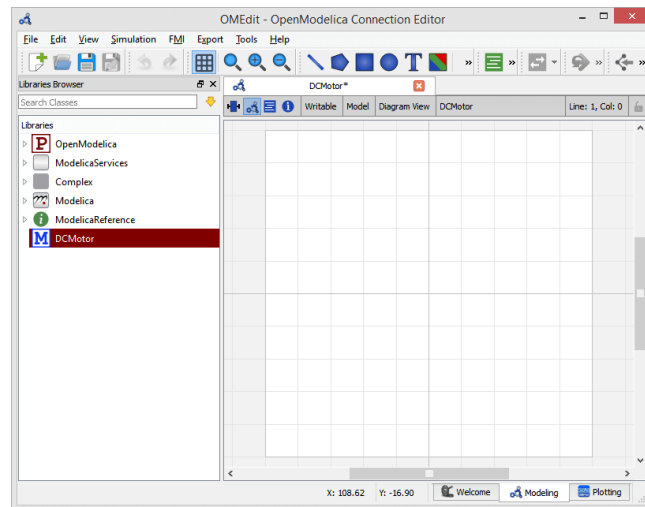


Fig. 5-1: OpenModelica Connection Editor (OME) modelling [37]

Modelling in OME is through connecting components from specific libraries and setting the correct parameters for the equations of each component and consequently of the model. It also offers modelling through code writing based on C++ [37]. Simulation results are in form of plots, as shown in fig. 5-2.

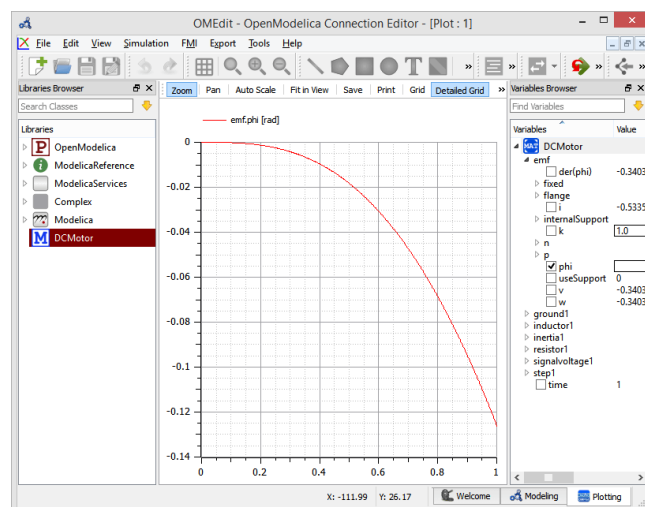


Fig. 5-2: OME plotting [37]

6 Modelling

As shown in fig. 6-1, the created overall model consists of a series of sub-models.

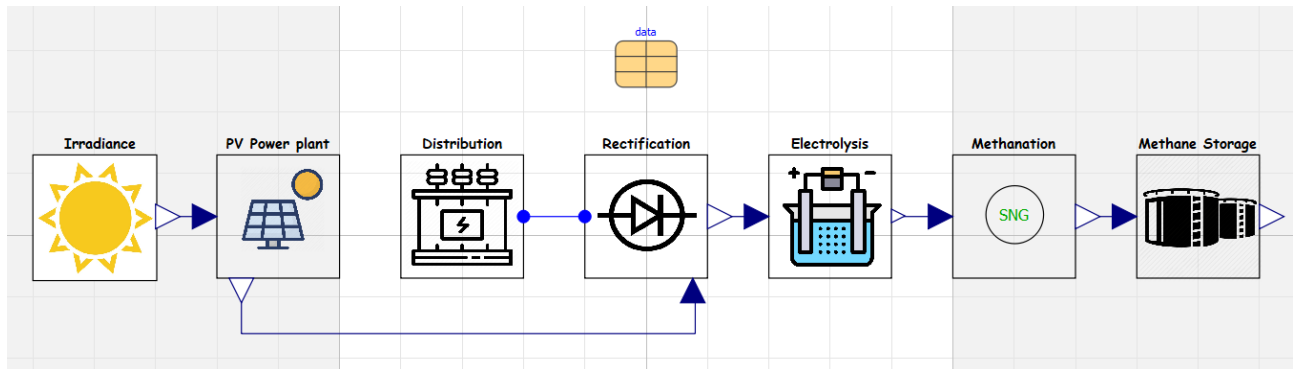


Fig. 6-1: Overall power-to-gas model

6.1 Electricity generation

Power-to-gas relies on electricity generated from renewable sources, namely solar and wind energy. In the model shown above, a solar power plant is considered.

6.1.1 Photovoltaic power plant

In the Irradiance sub-model, irradiance is detailed over a day, where the sun is considered to rise at 6:00 and set at 21:00, with peak irradiance being approximately around 13:30, reaching a maximum of 1000 W/m^2 . For simulation purposes, 86400 seconds in one day were taken in scale as 1 second. That is shown in fig. 6-2.

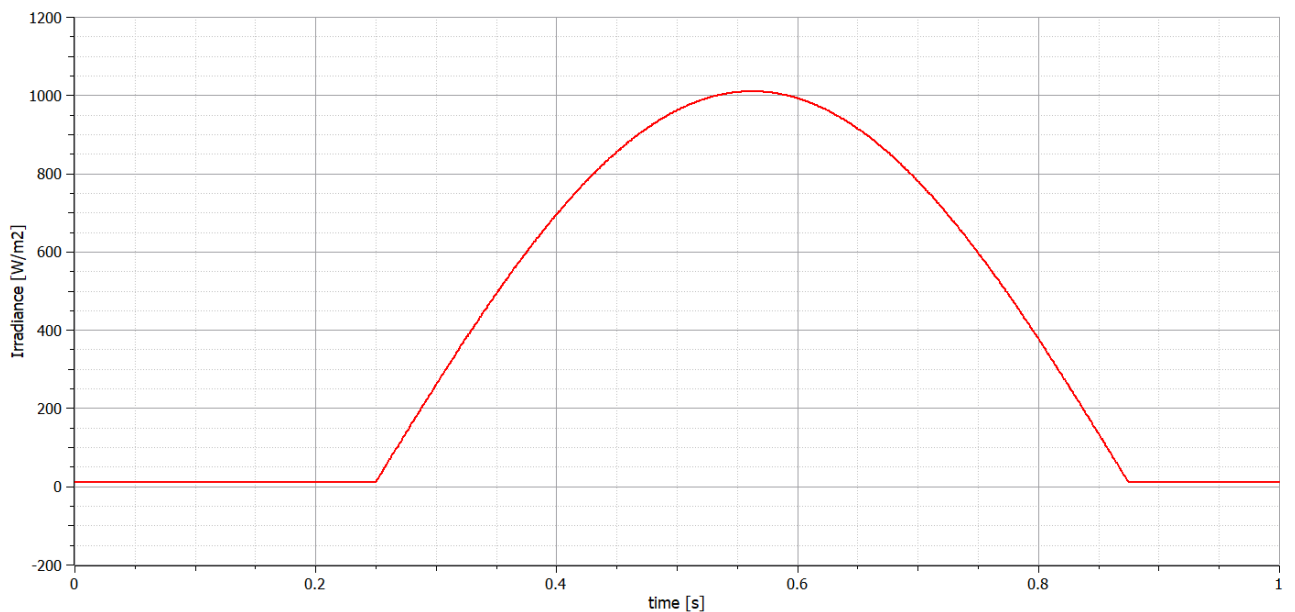


Fig. 6-2: Irradiance

Solar panels absorb solar power from sunlight to generate electricity. They are composed of solar cells which are a combination of photo-diodes. These panels can be set up in either series, parallel or serio-parallel connections to produce electricity in the form of DC current.

The PV power plant sub-model consists of a simple plant with the option of setting up the number of series and parallel connected panels. This is shown in fig. 6-3. The chosen panel for the model is a SHARP - NU-S5 (E3E)-185 W, it was chosen from a list of other panel models available in the Photovoltaics library.

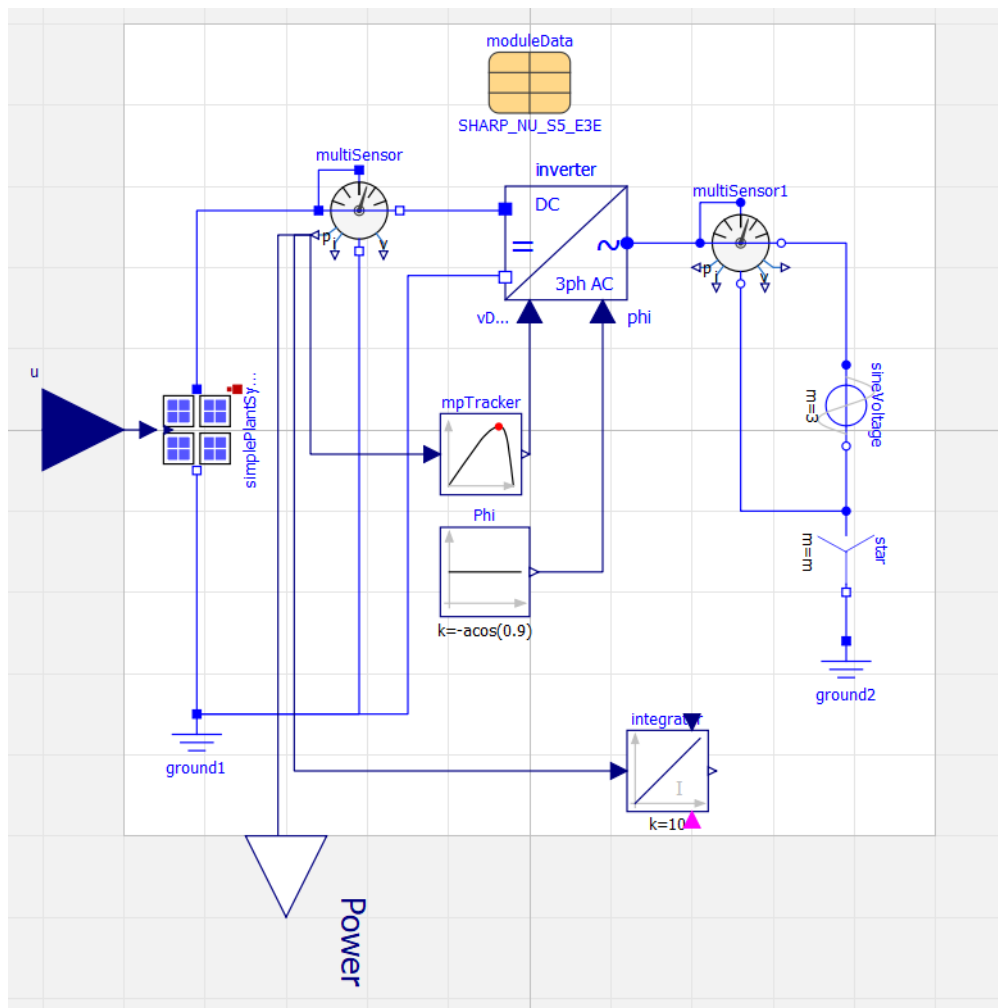


Fig. 6-3: PV power plant model

Tab. 6-1 lists the parameters of the used panels.

Tab. 6-1: SHARP - NU-S5 (E3E)-185W parameters at STC [38]

Maximum power	185	W_p
Open-circuit voltage	30.2	V
Short-circuit current	8.54	A
Voltage at maximum power point	24	V
Current at maximum power point	7.71	A
Efficiency	14.1	%

6.1.2 DC/AC inverter

A DC/AC inverter in the PV power plant sub-model converts the produced DC voltage to 3×400 V AC. The used inverter is considered to be ideal. This means losses are not considered. The AC output is determined based on power balance, calculated with instantaneous values:

$$V_{DC} \cdot I_{DC} + v_1 \cdot i_1 + v_2 \cdot i_2 + v_3 \cdot i_3 = 0 \quad (6.1)$$

where,

V_{DC} DC voltage from PV power plant [V]

v_1, v_2, v_3 Phase voltage [V]

i_1, i_2, i_3 Phase current [A]

The DC/AC inverter includes a Maximum Power Point Tracker (MPPT) to extract the power at maximum point. This is shown in fig. 6-4, to get the maximum power output of a PV panel, it needs to be operated at the maximum power point P_{MP} .

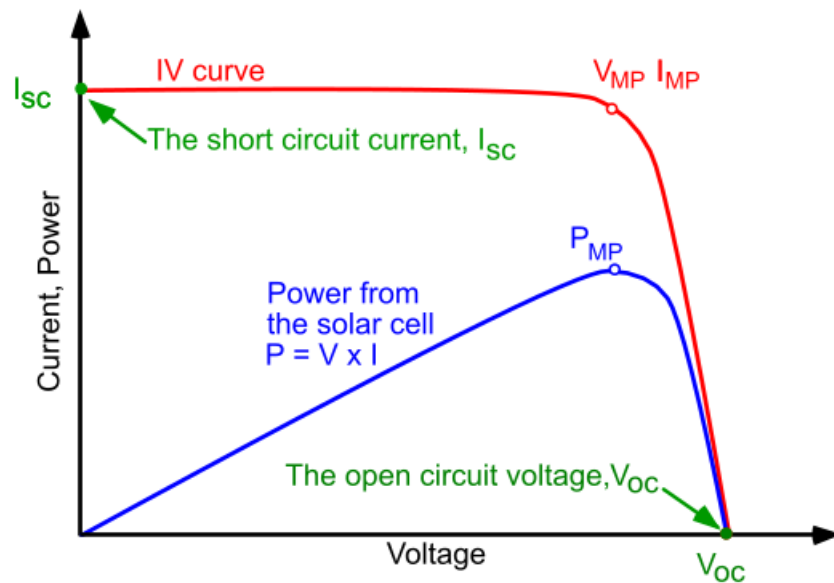


Fig. 6-4: IV curve of a solar cell [39]

6.1.3 Distribution and connection to the power grid

Transformers are used to transfer the electricity produced from the PV power plant. For purposes of modelling, the 400 V AC from the inverter is replaced with a SineVoltage source (see fig. 6-5). In a 3-step method, the 400 V AC from the inverter are transferred to be suitable for the load.

1. 400 V from is transferred to 22 kV through a 0.4/22 kV transformer.

2. This step could take two paths:

- (a) Path 1: From the 0.4/22 kV we directly feed the next transformer.
- (b) Path 2: From the 0.4/22 kV transformer, we can connect to the 22 kV MV network. The next transformer can be fed from the 22 kV MV level.

As shown in fig. 6-5, one of the two paths is chosen using a switch that either disconnects the 22 kV MV network (Path 1 - switch open) or connects the 0.4/22 kV transformer to the 22 kV MV network (Path 2 - switch closed). This is done in Openmodelica using a switch that takes a Boolean input (true \rightarrow switch closed, false \rightarrow switch open)

3. Through a step-down transformer, 22 kV is stepped-down to whatever voltage is needed, depending on the load.

In either case, the transferred voltage is then converted back to DC through a 6-pulse rectifier.

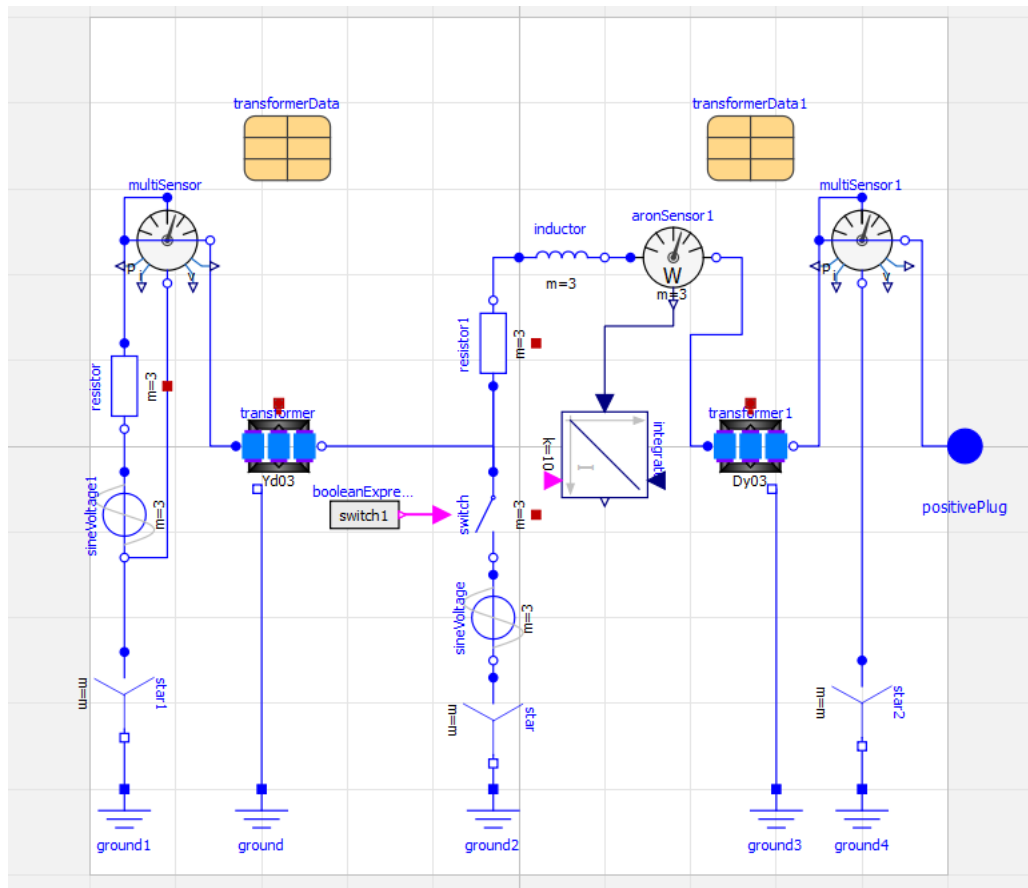


Fig. 6-5: Distribution model

The transmission lines for 22 kV are considered to be AlFe70 cables with a cross-sectional area $S = 70 \text{ mm}^2$, resistance $R = 0.4 \text{ } \Omega/\text{km}$ and inductive reactance $X = 0.35 \text{ } \Omega/\text{km}$ [40].

6.1.4 Rectification

As mentioned above, using a 6-pulse rectifier, the voltage is converted back to DC in order to feed the electrolyzers.

In the model, the rectifier sub-model has a power input that is fed from the PV power plant. That is used to determine the output current that feeds the electrolyzers, with a certain value of theoretical power loss considered through the inverter, transformers and transmission lines. This is also done to maintain correct values of power at all points of the model. Fig. 6-6 presents the rectification sub-model.

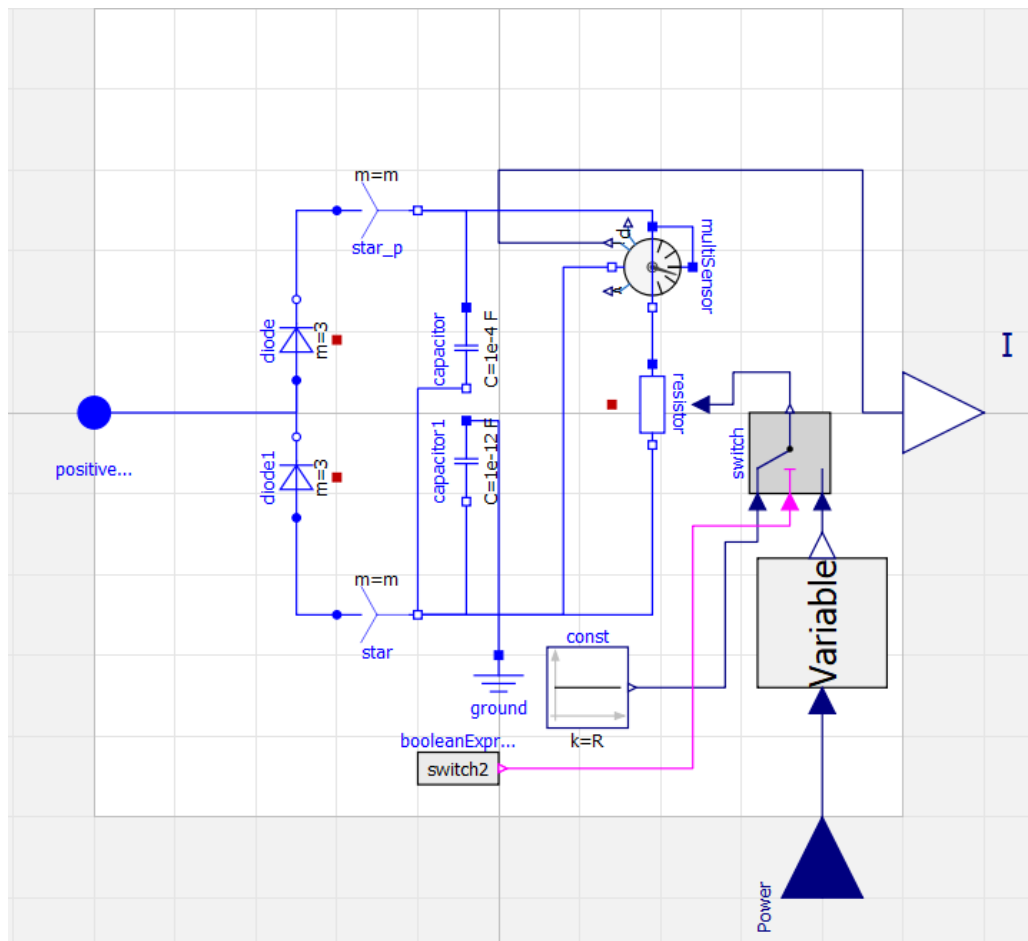


Fig. 6-6: Rectification model

In the case of Path 1, to obtain the correct shape of the current, which in this case depends on irradiance and power produced in the PV power plant, a resistor with variable resistance is used. While this isn't the case in real power-to-gas systems, but for purposes of modelling this was the best way to proceed.

In the case of Path 2, since the power is extracted from the 22 kV MV network without depending on the irradiance, a resistance with constant resistance (automatic setup depending on number of electrolyzers).

Just like in the Distribution sub-model, switching between paths is done using a binary switch that takes a Boolean input (true → constant resistance, false → variable resistance).

DC output voltage from the 3-phase rectifier is calculated as follows:

Peak phase to neutral voltage is:

$$V_{L-N(PEAK)} = \frac{V_{L-L}}{\sqrt{3}} \cdot \sqrt{2} \quad (6.2)$$

where,

$V_{L-N(PEAK)}$ Peak line to neutral voltage [V]

V_{L-L} Peak line-to-line voltage [V]

Then output DC voltage can be calculated according to [41]:

$$V_{DC} = V_{L-N(PEAK)} \cdot \frac{3 \cdot \sqrt{3}}{\pi} = V_{L-N(PEAK)} \cdot 1.654 \quad (6.3)$$

where,

V_{DC} DC output voltage [V]

DC output current from the 3-phase rectifier will consequently be:

$$I_{DC} = \frac{V_{DC}}{R} \quad (6.4)$$

where,

I_{DC} DC output current [A]

R Total load resistance [Ω]

6.2 Electrolysis

The electrolysis sub-model was taken from the model associated with [42]. The electrolyzer model is of an alkaline electrolysis cell (see sec. 2.3.1). The output DC current from the rectifier is used to feed the electrolyzers. The sub-model gives the option to set up the number of electrolyzers.

6.3 Methanation

6.3.1 Methanation reaction

In the model, catalytic methanation is considered. But due to the fact that, catalysts speed up the reaction, but are not consumed and don't appear in the product, the model doesn't include any catalyst. The reaction takes place under the following conditions: 400 °C (673.15 K) , 30 atm (3040 kPa) and $H_2:CO_2 = 4$ (see section. 4.2).



As seen in the fig. 6-7, the input into the reaction is the hydrogen feed. Hydrogen, being the limiting reactant, sets the feed of CO₂ into the reaction.

$$V_{\text{H}_2} \cdot \rho_{\text{H}_2} = m_{\text{H}_2} \quad (6.6)$$

$$\frac{m_{\text{H}_2} \cdot 1000}{M_{\text{H}_2}} = n_{\text{H}_2} \quad (6.7)$$

where,

V_{H_2} Volume of H₂ feed [m³]

n_{H_2} Number of moles of H₂ [mol]

m_{H_2} Mass [kg]

ρ_{H_2} Density [kg/m³], the value of ρ_{H_2} is 0.08375 kg/m³

M_{H_2} Molar mass of H₂ [g/mol], the value of M_{H_2} is 2.016 g/mol

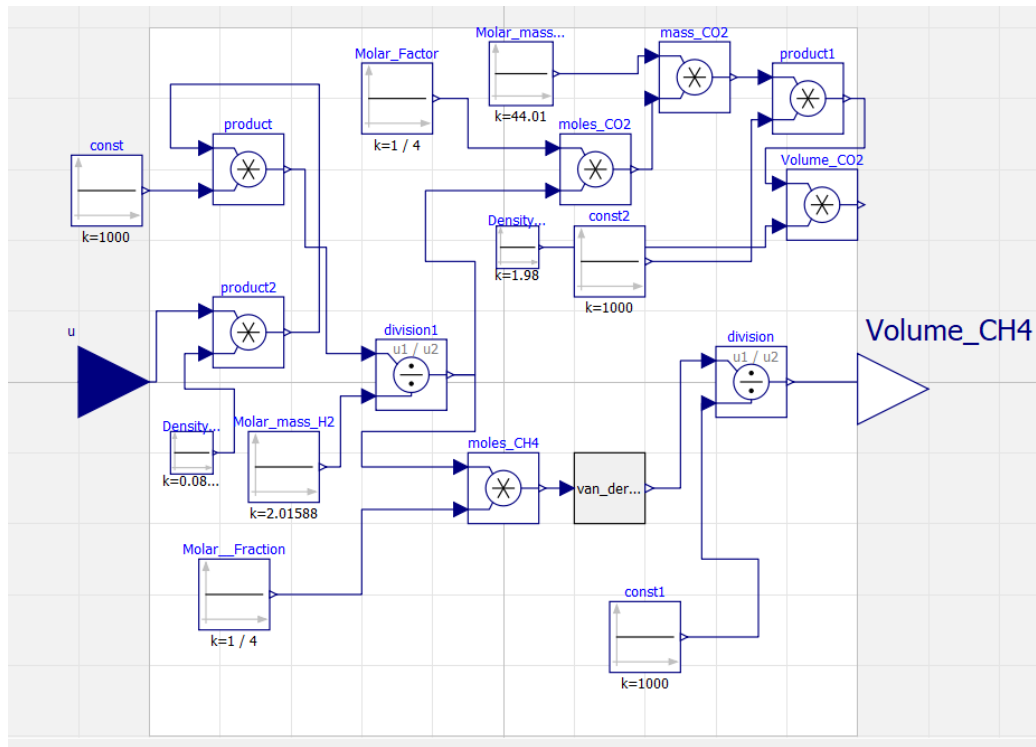


Fig. 6-7: Methanation model

To find the volume of CO₂ needed, the number of moles is calculated using the molar fraction $\text{H}_2/\text{CO}_2 = 4$.

$$n_{\text{H}_2} \cdot \frac{1}{4} = n_{\text{CO}_2} \quad (6.8)$$

$$n_{\text{CO}_2} \cdot \frac{M_{\text{CO}_2}}{1000} = m_{\text{CO}_2} \quad (6.9)$$

$$\frac{m_{\text{CO}_2}}{\rho_{\text{CO}_2}} = V_{\text{CO}_2} \quad (6.10)$$

where,

- n_{CO_2} Number of moles of CO_2 [mol]
- V_{CO_2} Volume of CO_2 feed [m^3]
- m_{CO_2} Mass [kg]
- ρ_{CO_2} Density [kg/m^3], the value of ρ_{CO_2} is $1.98 \text{ kg}/\text{m}^3$
- M_{CO_2} Molar mass of CO_2 [g/mol], the value of M_{CO_2} is $44.01 \text{ g}/\text{mol}$

Similarly, the number of moles of CH_4 is produced is calculated.

$$n_{\text{H}_2} \cdot \frac{1}{4} = n_{\text{CH}_4} \quad (6.11)$$

where,

- n_{CH_4} Number of moles of CH_4 [mol]

6.3.2 Van der Waals equation

Van der Waals equation is an equation that takes into consideration the fact that real gases deviate from the assumptions taken for ideal gases, especially at low temperatures or high pressures [43].

Using Van der Waals equation, the volume of the produced methane is calculated.

$$\left(p + \frac{an^2}{V^2}\right)(V - nb) = nRT \quad (6.12)$$

According to [44], to calculate V from van der Waals equation, the V in $\frac{an^2}{V^2}$ can be approximated as $\frac{nRT}{p}$.

Then V is calculated as:

$$V = \frac{nR^3T^3}{pR^2T^2 + ap^2} + nb \quad (6.13)$$

where,

- R Ideal gas constant, the value of R is $0.0821 \text{ atm} \cdot \text{L} \cdot \text{mol}^{-1} \cdot \text{K}^{-1}$
- a, b Constants, in the case of CH_4 $a = 2.2678 \text{ atm} \cdot \text{L}^2/\text{mol}^2$ and $b = 0.04301 \text{ L}/\text{mol}$
- p Pressure [atm]
- T Temperature [K]

n Number of moles [mol]

V Volume [L]

The following model in fig. 6-8 presents the van der Waals equation.

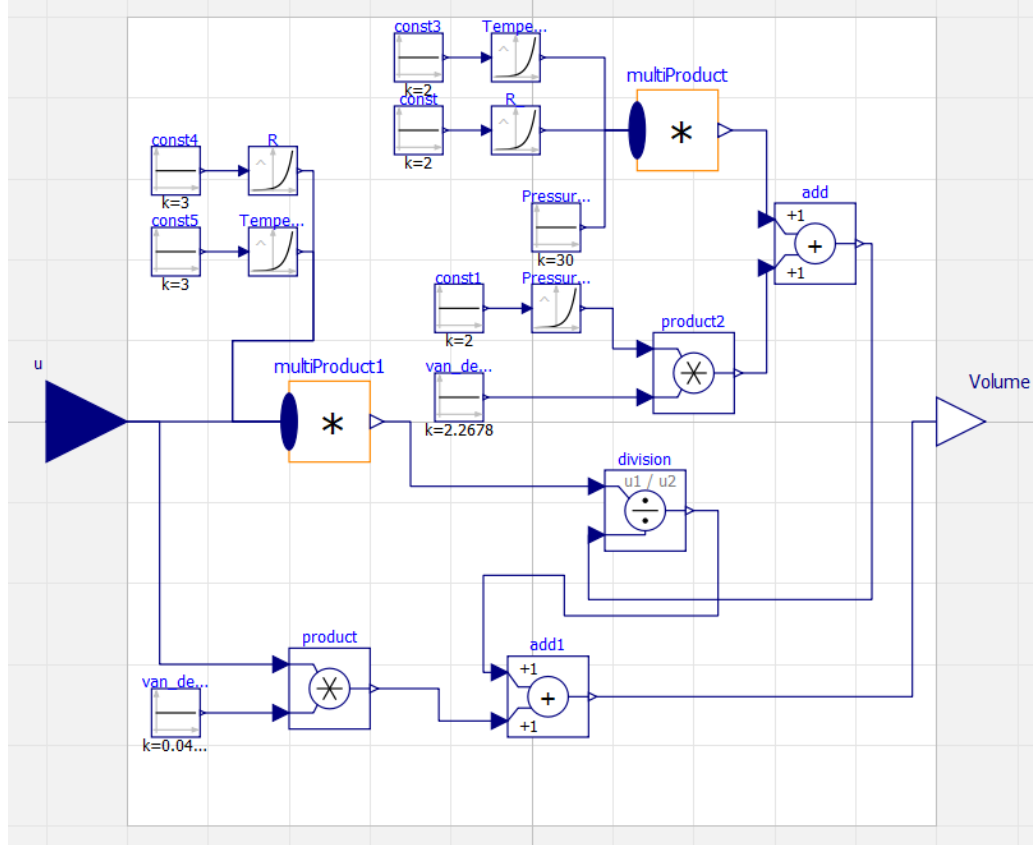


Fig. 6-8: Van der Waals equation model

6.3.3 Methane production and storage

The produced methane is accumulated and stored in tanks. To calculate the energy produced at STP, we use the heat of combustion of methane. But first we need to convert the amount of methane produced in m^3 to Nm^3 because methanation takes place under temperatures and pressures different from STP 0°C (273.15 K) and 1 atm (101.325 kPa). In our case, methanation was considered to take place at 400°C (673.15 K) and 30 atm (3040 kPa).

$$\frac{V_1 \cdot p_1}{T_1} = \frac{V_2 \cdot p_2}{T_2} \quad (6.14)$$

$$\frac{V_1 \cdot 3.04 \cdot 10^6}{673.15} = \frac{V_2 \cdot 1.01325 \cdot 10^5}{273.15} \quad (6.15)$$

$$V_2 = \frac{V_1 \cdot 3.04 \cdot 10^6}{673.15} \cdot \frac{273.15}{1.01325 \cdot 10^5} \quad (6.16)$$

where,

V_1 Volume [m^3]

V_2 Volume [Nm^3]

p_1 Pressure [Pa]

p_2 Pressure [Pa]

T_1 Temperature [K]

T_2 Temperature [K]

According to [45], the heat of combustion of methane at STP is 38819 kJ/Nm^3 . Then the energy equivalent would be:

$$E = \frac{V_{\text{CH}_4} \cdot H}{3600} \quad (6.17)$$

where,

E Energy [kWh]

V_{CH_4} Volume of methane produced [Nm^3]

H Heat of combustion of methane [kJ/Nm^3]

Heat of combustion is the amount of heat that is released by the ideal combustion of a certain amount of fuel. It is assumed that the water released by combustion condenses and the energy of the chemical reaction does not need to be reduced by its latent heat. This makes the heat of combustion different from the calorific value, where gaseous water is assumed at the end of the reaction. Therefore, the value of the heat of combustion is always greater than or equal to the value of the calorific value. They're equal when combustion does not produce water [46].

The accumulation of methane model was simply done using an integrator. It calculated the total volume of methane produced and stored.

6.4 Simulation

For purposes of analysis and to test the functionality of the model, a simulation was carried out. As stated above, distribution could take one of two paths. For every path, a separate simulation and its corresponding results were taken.

The simulation was realized with the following parameters (fig. 6-9):

Photovoltaic power plant	
nS	30 Number of series connected panels
nP	2 Number of parallel connected panels
DC/AC Converter	
VRef	400 V Reference line to line voltage
f	50 Hz Frequency
Ti	0.00154 s Internal integration time constant
Transformers	
V1prim	400 / sqrt(3) V Primary RMS phase voltage - step-up transformer
V1sec	22E3 V Secondary phase voltage - step-up transformer
V2prim	22E3 V Primary phase voltage - step-down transformer
Sn	50E3 V.A Nominal apparent power
v_sc	0.04 Impedance voltage drop pu
P_sc	1100 W Short-circuit (copper) losses
l	50E3 m MV cable length
Electrolyzer	
NumberOfElectrolyzers	35 Number of Electrolyzers
NumberOfElectrodes	2 Number of Electrodes

Fig. 6-9: Simulation parameters

Path 1: The step-down transformer is directly fed from the 0.4/22 kV transformer.

1. Power from PV power plant:

At MPP, the power from the PV power plant reaches 11102.4 W. This is illustrated in the equations eq. 6.18, eq. 6.19, eq. 6.20 and fig. 6-10.

$$V = n_{series} \cdot 24 = 30 \cdot 24 = 720 \text{ V} \quad (6.18)$$

where,

n_{series} Number of series connected panels.

$$I = n_{parallel} \cdot 7.71 = 2 \cdot 7.71 = 15.42 \text{ A} \quad (6.19)$$

where,

$n_{parallel}$ Number of parallel connected panels.

$$P = V \cdot I = 720 \cdot 15.42 = 11102.4 \text{ W} \quad (6.20)$$

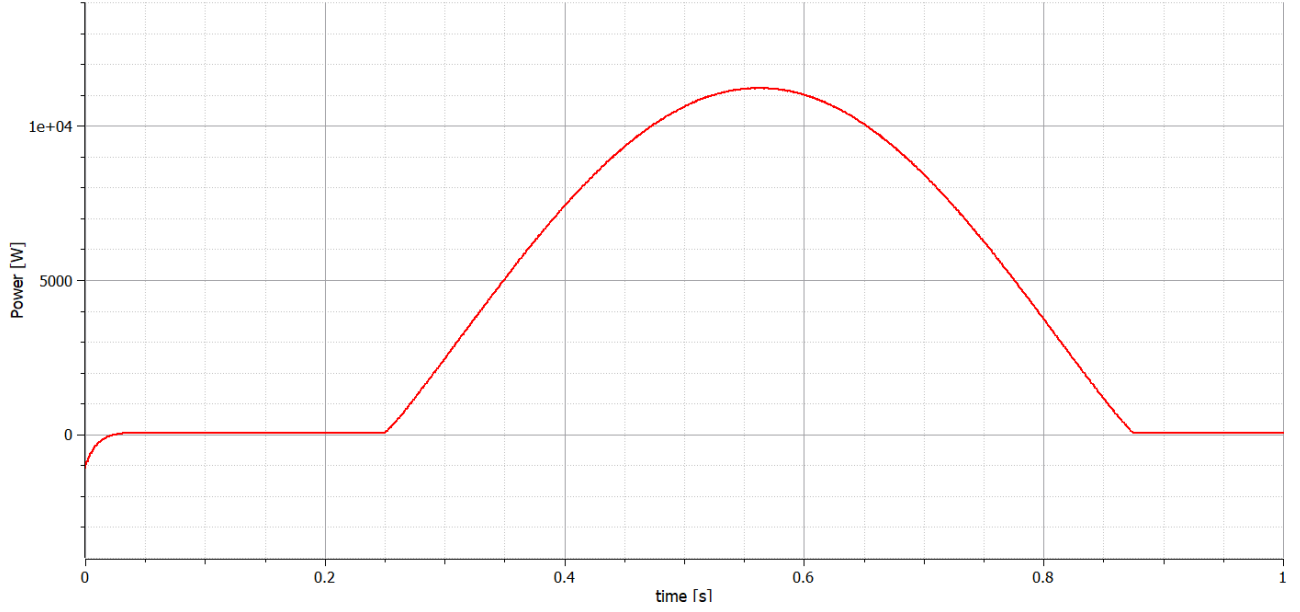


Fig. 6-10: Generated power

2. Step-down transformer and rectification:

After transferring the 400 V to 22 kV, the next transformer steps down the voltage to the needed value according to the load. This voltage is then connected to the 6-pulse rectifier.

Considering that the voltage of one AEC is around 2 V (see tab. 2-2). The needed DC voltage to power the 35 electrolyzers is:

$$V_{DC} = 2 \cdot n_{electrolyzers} = 2 \cdot 35 = 70 \text{ V} \quad (6.21)$$

where,

$n_{electrolyzers}$ Number of series connected electrolyzers

According to sec. 6.1.4:

$$V_{DC} = V_{L-N(PEAK)} \cdot 1.654 \quad (6.22)$$

Then,

$$V_{L-N(PEAK)} = \frac{V_{DC}}{1.654} = \frac{70}{1.654} = 42.32 \text{ V} \quad (6.23)$$

Consequently,

$$V_{L-L(PEAK)} = V_{L-N(PEAK)} \cdot \sqrt{3} = 42.32 \cdot \sqrt{3} = 73.3 \text{ V} \quad (6.24)$$

The DC current has the following graph:

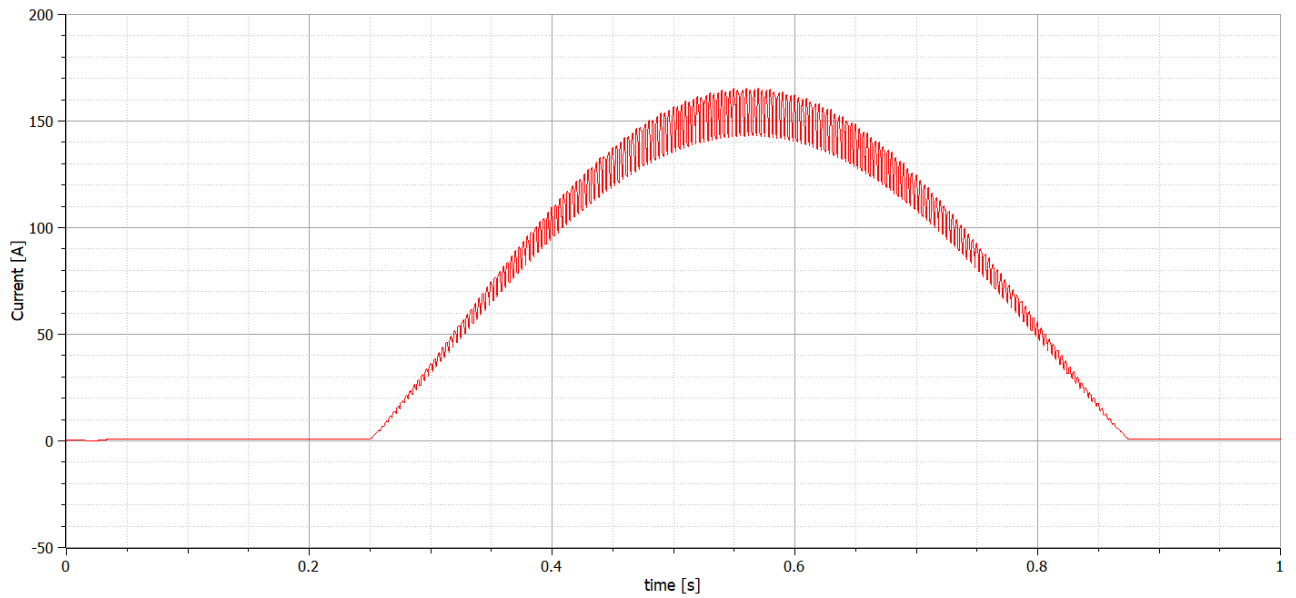


Fig. 6-11: DC current

It is clear in fig. 6-11 that the current increases with increasing power and decreases as so.

3. Electrolysis:

The following graph shows the produced volume of H₂ that consequently is fed into the methanation reactor for further reaction with CO₂ (fig. 6-12).

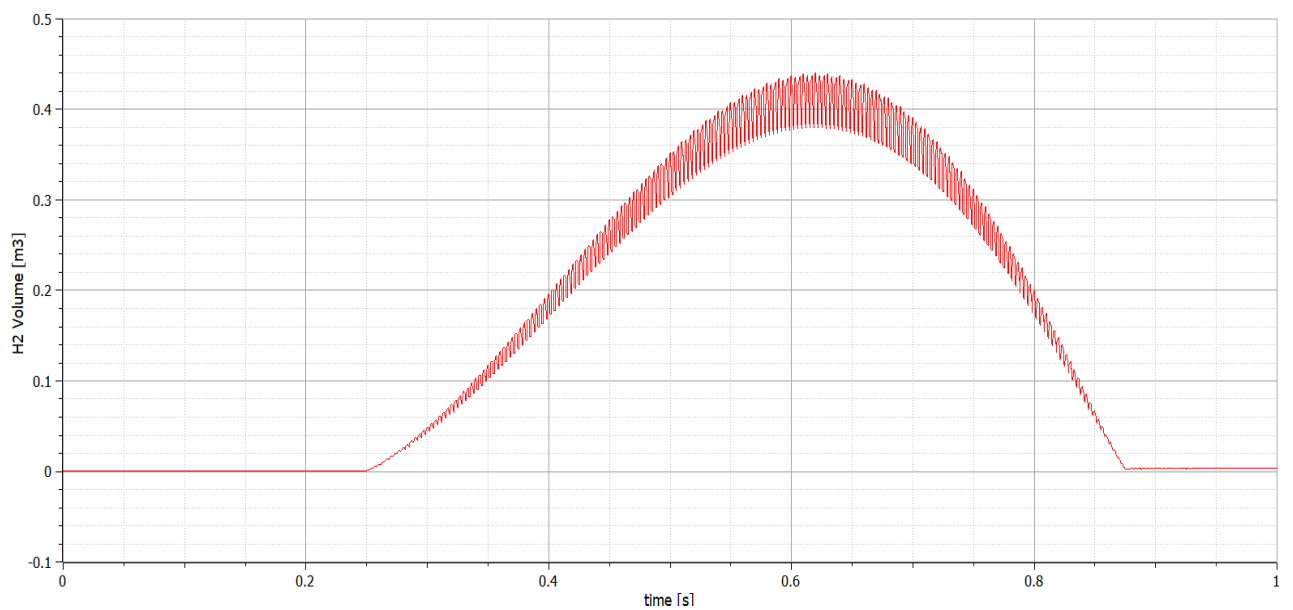


Fig. 6-12: Hydrogen production

4. Methanation and storage:

The volume of the produced methane is calculated using van der Waals equation for real gases (see sec. 6.3.2). Fig. 6-13 shows the production of methane.

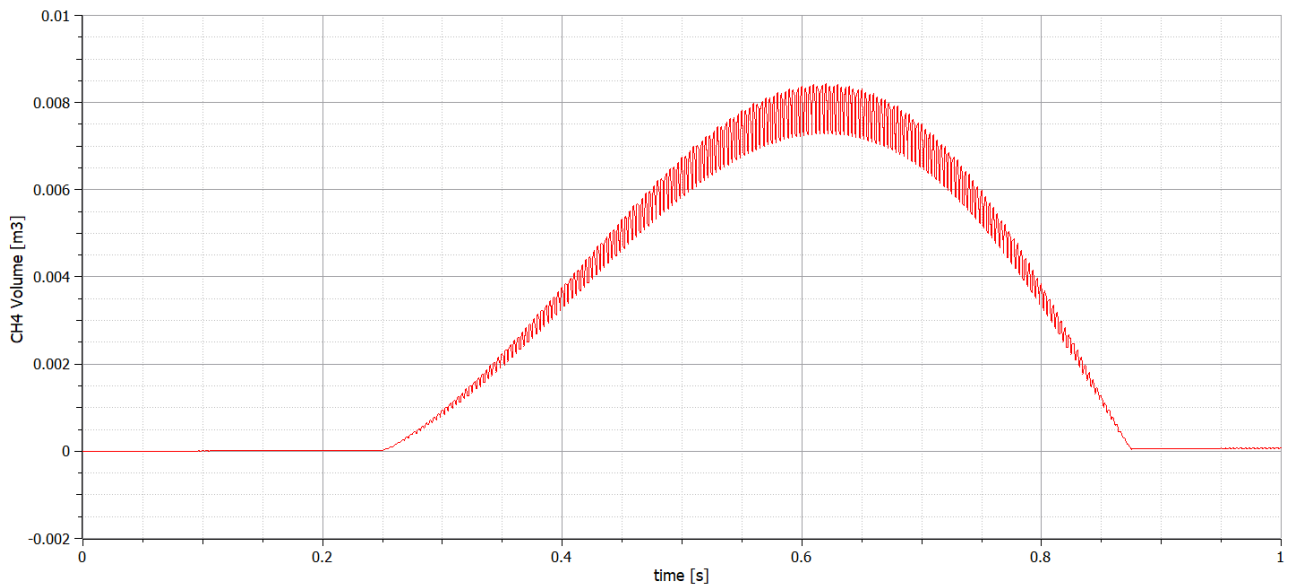


Fig. 6-13: Methane production

Consequently, the produced methane is stored in tanks. The following fig. 6-14 shows the accumulated volume of methane.

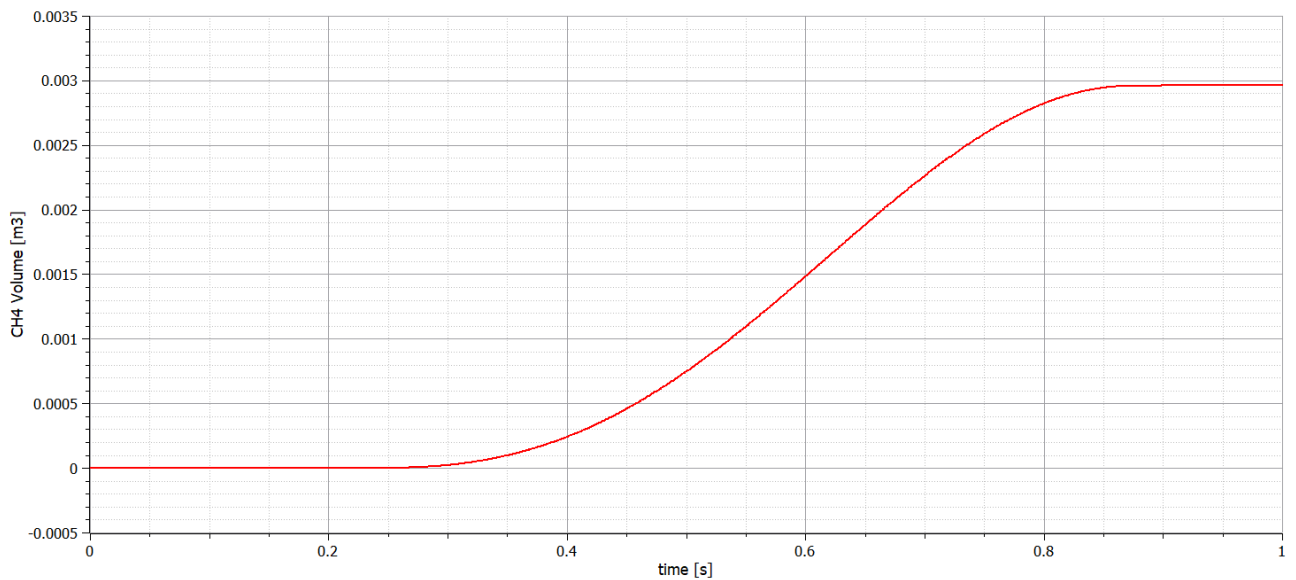


Fig. 6-14: Methane accumulation

5. Efficiency

The efficiency of the system is calculated with the input and output energy. Input energy being the power generated over the course of a day. Output energy is calculated from the produced methane.

The input energy from the PV power plant was 5.7 kWh. As for the output energy, it is calculated according to eq. 6.17. But first the volume of methane produced is converted from m^3 to Nm^3 . Using eq. 6.16:

$$V_{\text{CH}_4} = \frac{0.0029 \cdot 3.04 \cdot 10^6}{673.15} \cdot \frac{273.15}{1.01325 \cdot 10^5} = 0.035 \text{ Nm}^3 \quad (6.25)$$

$$E = \frac{V_{\text{CH}_4} \cdot \Delta H}{3600} = \frac{0.035 \cdot 38819}{3600} = 0.38 \text{ kWh} \quad (6.26)$$

$$\eta = \frac{E_{\text{CH}_4}}{E_{\text{PV}}} = \frac{0.38}{5.7} = 6.62\% \quad (6.27)$$

Since the system is operating with a photovoltaic power plant, it's possible to calculate one more efficiency with the input energy being the energy from sunlight. From fig. 6-2 and the structure of the chosen panel, we can know how much energy in kWh did the PV power plant receive and therefore have a more precise efficiency of the system as a whole.

The used panels in the PV power plant sub-model (see. tab. 6-1) have 48 cells, each has surface area $156 \times 156 \text{ mm}$. With the simulation parameters mentioned above (see fig. 6-9).

Surface area of one panel:

$$A_{\text{panel}} = n_{\text{cells}} \cdot A_{\text{cell}} = 48 \cdot (156 \cdot 10^{-3})^2 = 1.17 \text{ m}^2 \quad (6.28)$$

where,

A_{panel} Surface area of a panel [m^2]

n_{cells} Number of cells in a panel

A_{cell} Surface area of one cell [m^2]

Total surface area of connected solar panels:

$$A_{\text{tot}} = n_{\text{panels}} \cdot A_{\text{panel}} = 60 \cdot 1.17 = 70.2 \text{ m}^2 \quad (6.29)$$

where,

A_{tot} Total surface area [m^2]

n_{panels} Number of panels in power plant

Over the course of a day, the panels receive a total of 0.408 kWh/m^2 .

Then the total input energy is:

$$E_{\text{solar}} \cdot A_{\text{tot}} = 0.408 \cdot 70.2 = 28.64 \text{ kWh} \quad (6.30)$$

where,

E_{solar} Solar energy from sunlight [kWh]

The output energy from the PV power plant in Path 1 is 5.7 kWh.
To verify the panel efficiency in tab. 6-1:

$$\eta_{panel} = \frac{E_{PV}}{E_{irradiance}} = \frac{5.7}{28.64} = 19.9\% \quad (6.31)$$

This is in the expected range.

$$\eta = \frac{E_{CH_4}}{E_{irradiance}} = \frac{0.38}{28.64} = 1.32\% \quad (6.32)$$

It is clear that the efficiency in this case is relatively very low, this is mainly due to the low efficiency of the PV panels leading to high power loss.

Path 2: The step-down transformer is fed from the 22 kV MV network. Now the input power is taken for the whole day and is not dependent on the PV power plant and irradiance.

1. Power from 22 kV MV network:

The extracted power from the 22 kV MV network is initially fed from the PV power plant. The difference in this path is that the power is now continuously extracted from the MV network without any alteration or dependence on solar irradiance. Fig. 6-15 shows the active power extracted from the MV network.

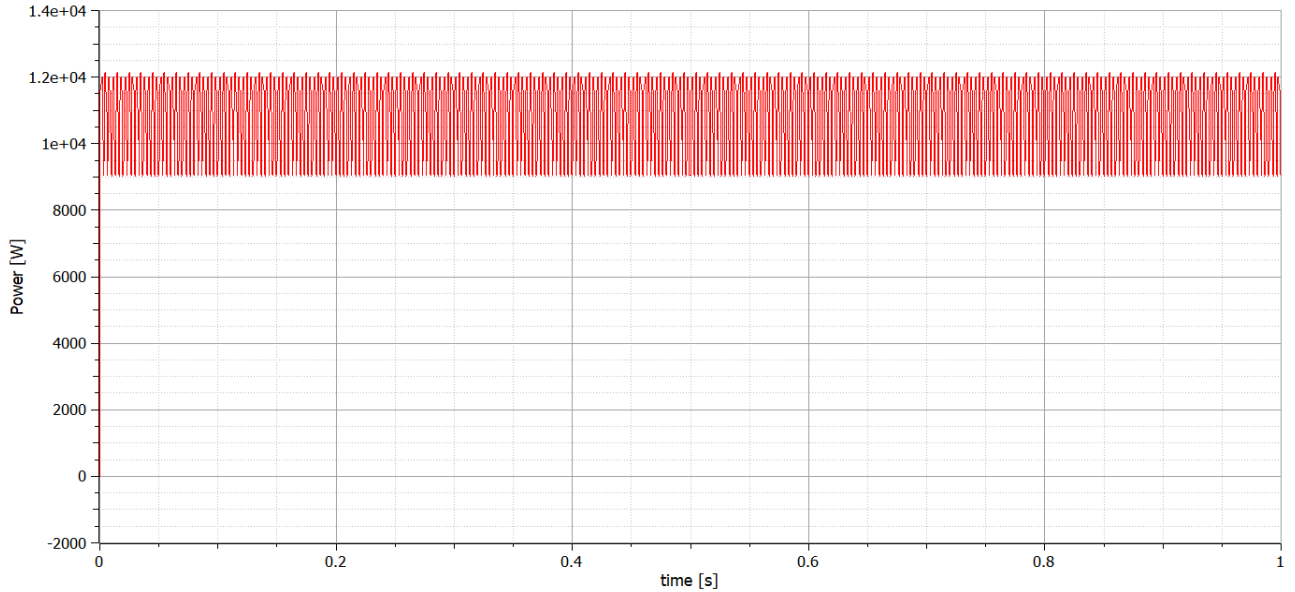


Fig. 6-15: Active power from 22 kV MV network

2. Rectification:

The DC current feeding the electrolyzers is presented in fig. 6-16. The AC voltage to power the rectifier and consequently output the needed voltage for the electrolyzers is the same as in Path 1. But since the power in this case is continuously extracted without any modifications, the DC current from the rectifier is constant.

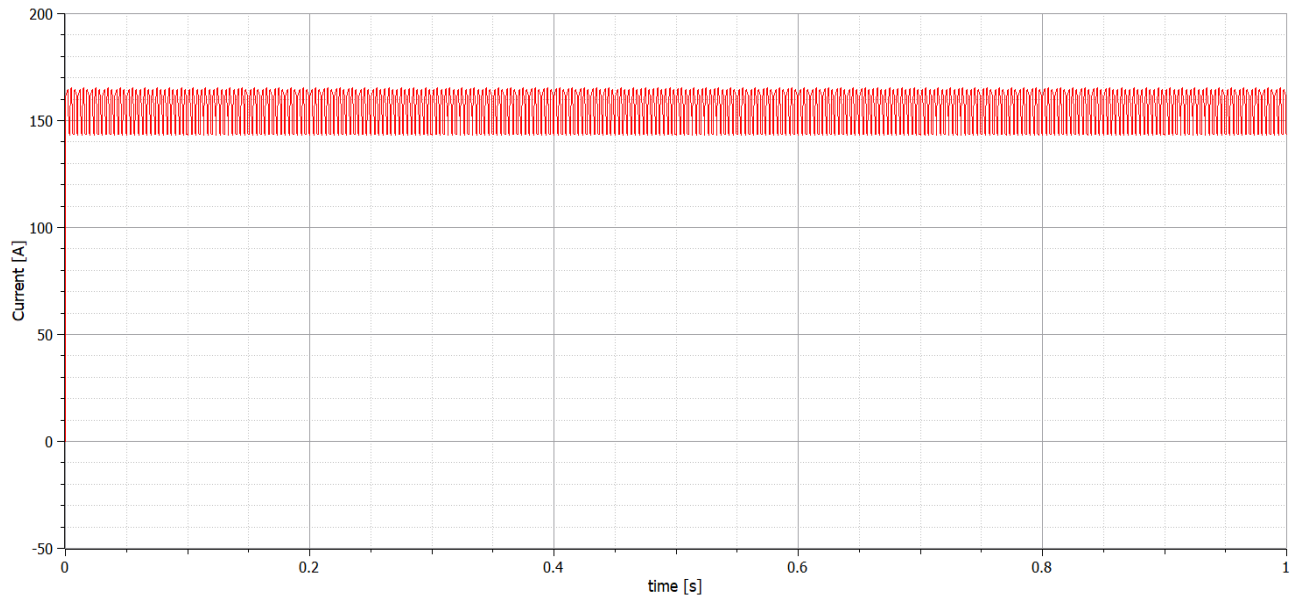


Fig. 6-16: DC current

3. Electrolysis:

As mentioned above, the current feeding the electrolyzers is in this case constant, this means the production of hydrogen will linearly increase with time. This is shown in fig. 6-17.

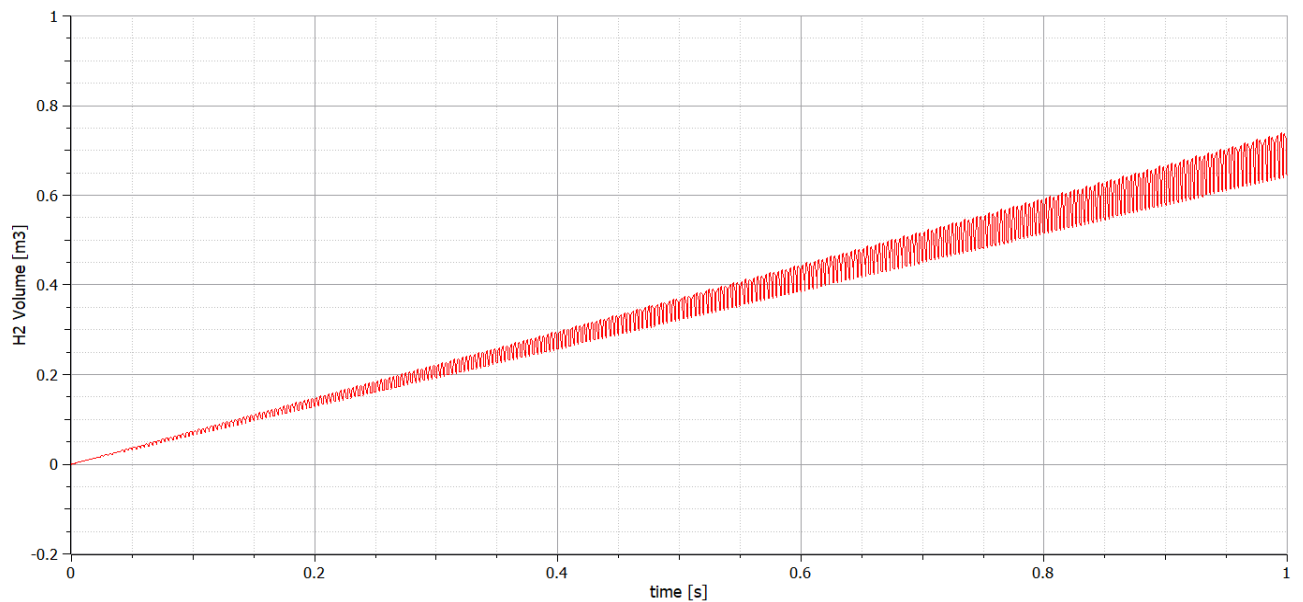


Fig. 6-17: Hydrogen production

4. Methanation and storage:

Again using van der Waals equation for real gases, the volume of the produced methane is calculated. Fig. 6-18 shows the production of methane.

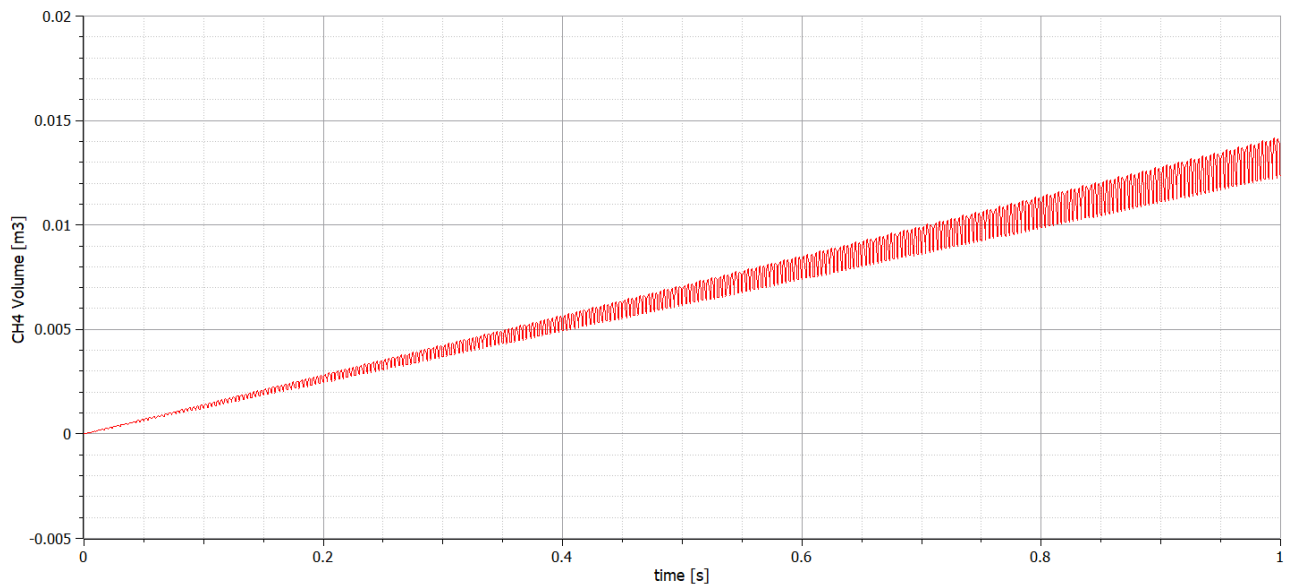


Fig. 6-18: Methane production

Fig. 6-19 shows the accumulation of methane.

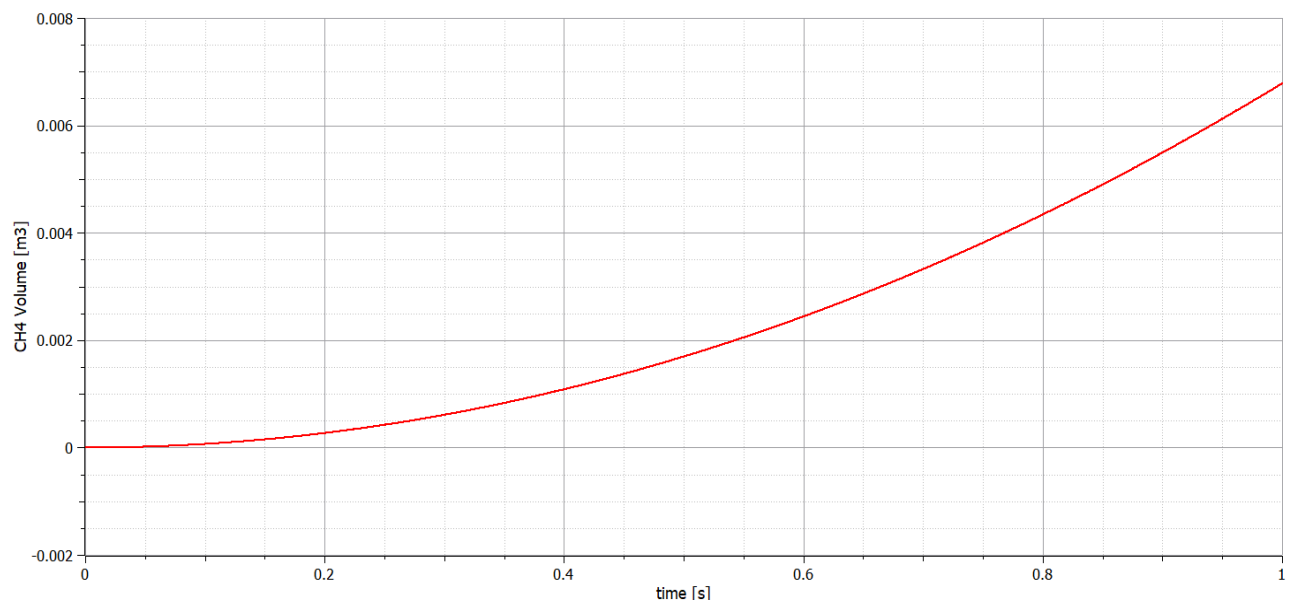


Fig. 6-19: Methane accumulation

5. Efficiency

The efficiency of the system is calculated with the input and output energy. The input energy in this case is the active power extracted from the MV network over the course of a day. Output energy is calculated from the produced methane.

The input energy was 11.05 kWh. The output energy is calculated according to eq. 6.17.

$$V_{\text{CH}_4} = \frac{0.0068 \cdot 3.04 \cdot 10^6}{673.15} \cdot \frac{273.15}{1.01325 \cdot 10^5} = 0.083 \text{ Nm}^3 \quad (6.33)$$

$$E = \frac{V_{\text{CH}_4} \cdot \Delta H}{3600} = \frac{0.083 \cdot 38819}{3600} = 0.895 \text{ kWh} \quad (6.34)$$

$$\eta = \frac{E_{\text{CH}_4}}{E_{\text{network}}} = \frac{0.895}{11.05} = 8.1 \% \quad (6.35)$$

6.5 Energy storage in batteries

For purposes of comparison, another model consisting of the same electricity generation sub-models but instead of electrolysis and methanation, a batteries sub-model connected. Fig 6-20 presents the overall batteries model.

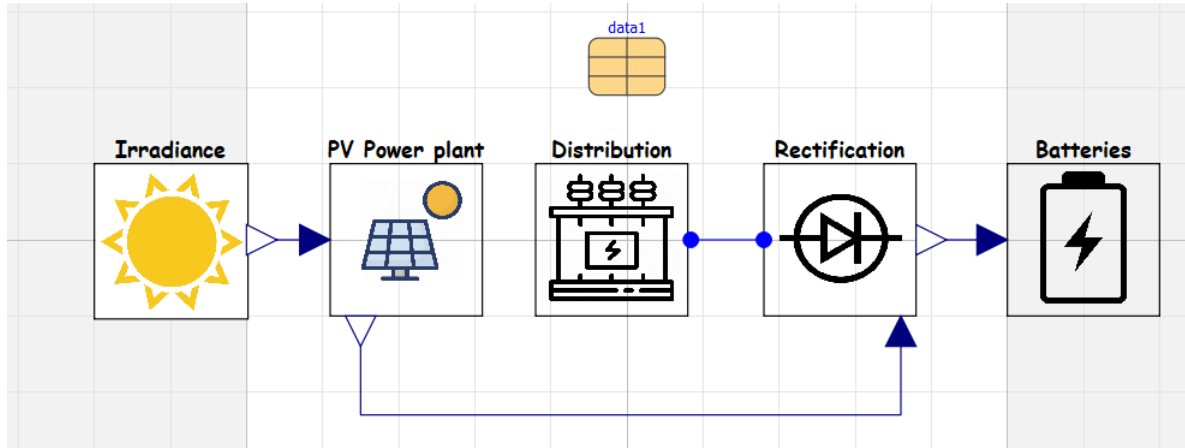


Fig. 6-20: Batteries model

Fig. 6-21 presents the batteries model, it includes the battery stack with an option to set the number of series batteries and parallel batteries. It also includes battery parameters like charge capacity, capacitance, resistance, and SOCOCV table. The component SignalCurrent was used to take the output current from the rectifier and regenerate it into the batteries circuit.

Just like in the case of P2G, the output DC current from the rectifier sub-model is either constant or variable, depending on the path. That is done by switching between constant and variable resistance. Since the simulation was limited to 1 second due to complications, charge capacity was set to $Q = 115 \text{ C}$ in order to potentially fully charge in 1 s.

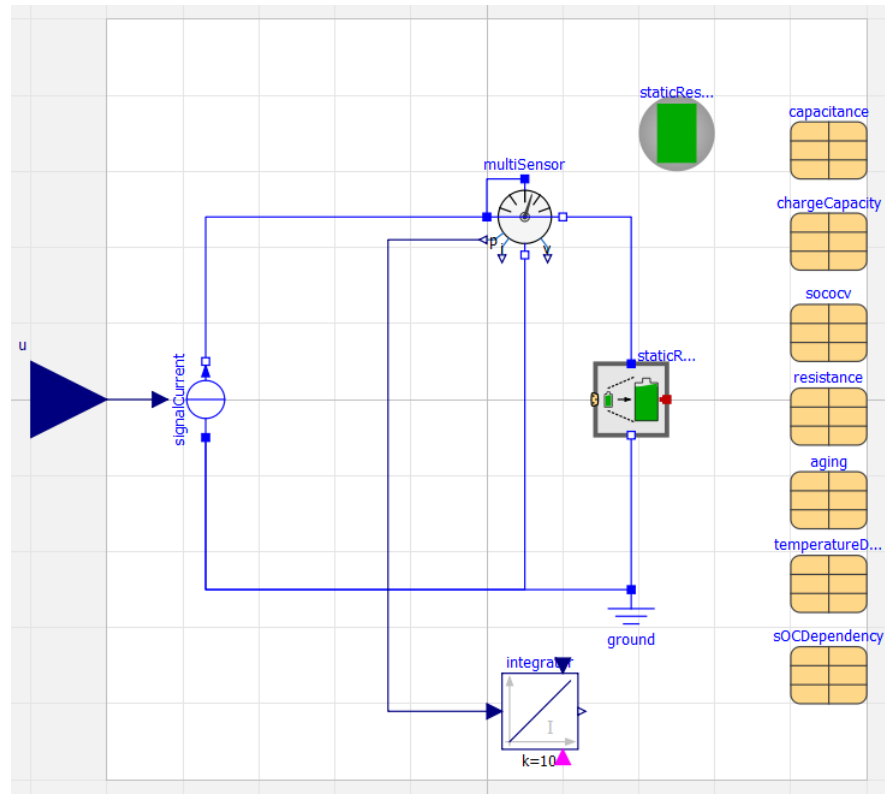


Fig. 6-21: Batteries model

The following are the simulation parameters (fig. 6-22):

Photovoltaic power plant		
nS	30	Number of series connected panels
nP	2	Number of parallel connected panels
DC/AC Converter		
VRef	400	V Reference line to line voltage
f	50	Hz Frequency
Ti	0.00154	s Internal integration time constant
Transformers		
V1prim	400 / sqrt(3)	V Primary RMS phase voltage - step-up transformer
V1sec	22E3	V Secondary phase voltage - step-up transformer
V2prim	22E3	V Primary phase voltage - step-down transformer
Sn	50E3	V.A Nominal apparent power
v_sc	0.04	Impedance voltage drop pu
P_sc	1100	W Short-circuit (copper) losses
l	50E3	m MV cable length
Battery Stack		
Ns	25	Number of series cells connected
Np	1	Number of parallel cells connected

Fig. 6-22: Simulation parameters

Again, two paths are examined:

Path 1:

DC output current from rectifier is shown in fig. 6-23:

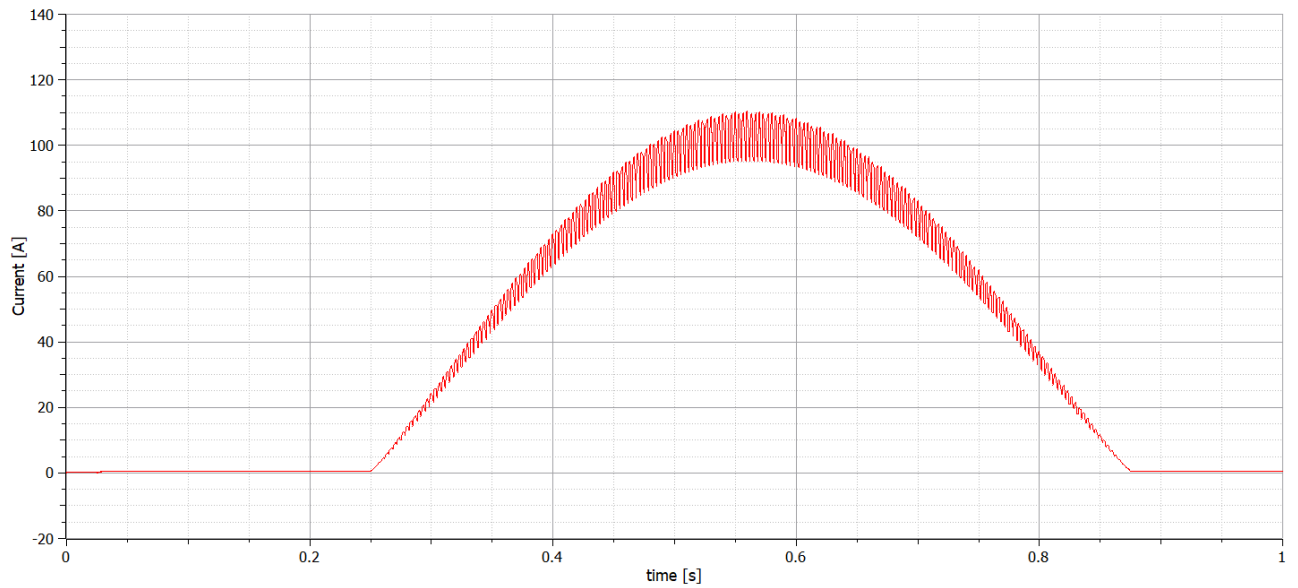


Fig. 6-23: DC current

The batteries are not fully charged due to the variable current. State of charge is shown in fig. 6-24:

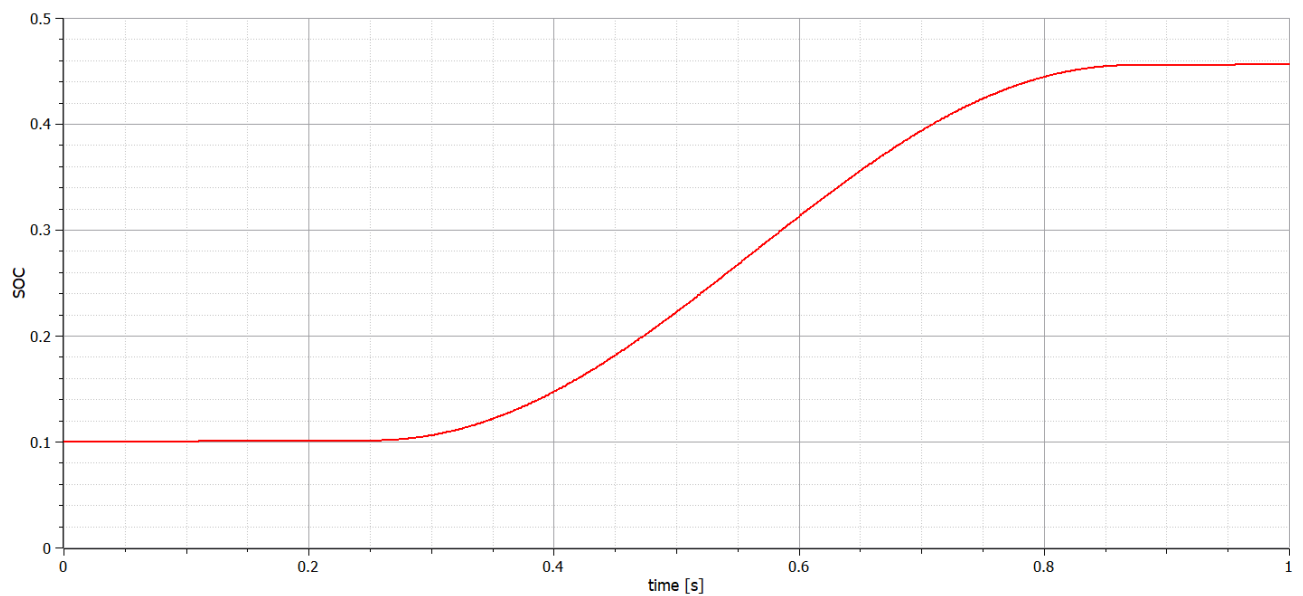


Fig. 6-24: State of charge (SOC)

The energy stored in the batteries is present in fig. 6-25:

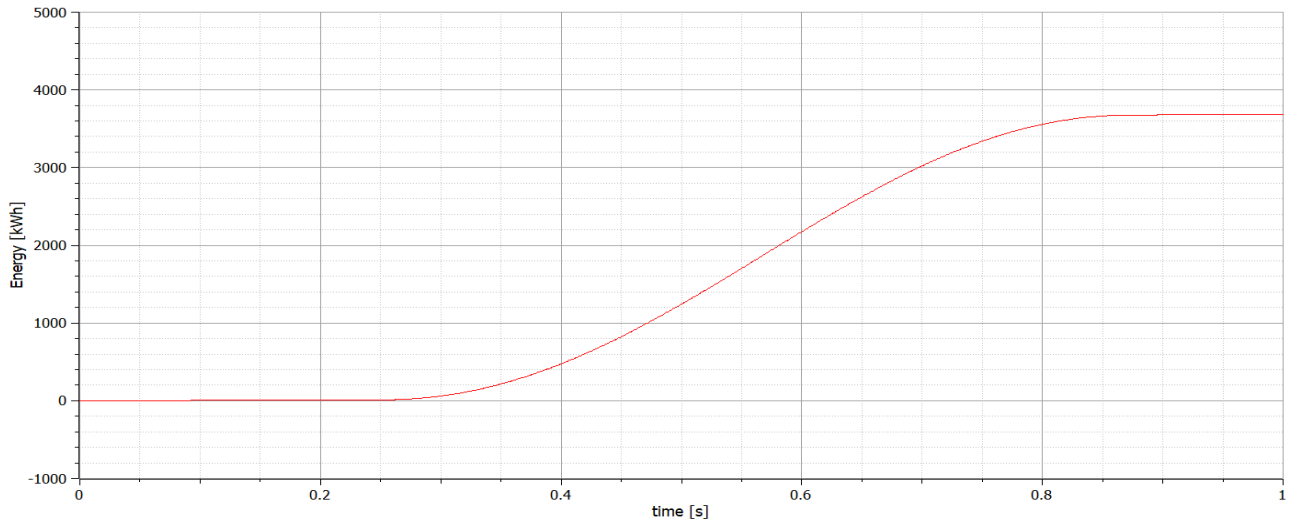


Fig. 6-25: Energy

The efficiency of the system is calculated with the input and output energy. The input energy is that of the PV power plant $E_{PV} = 5.7 \text{ kWh}$

$$\eta = \frac{E_{\text{batteries}}}{E_{PV}} = \frac{3.68}{5.7} = 64.56\% \quad (6.36)$$

Again, taking into account the efficiency of the panels, we calculate a more precise efficiency of the system as a whole.

Using eq. 6.32:

$$\eta = \frac{E_{\text{batteries}}}{E_{\text{irradiance}}} = \frac{3.68}{28.64} = 12.85\% \quad (6.37)$$

Path 2:

DC output current from rectifier is shown in fig. 6-26.

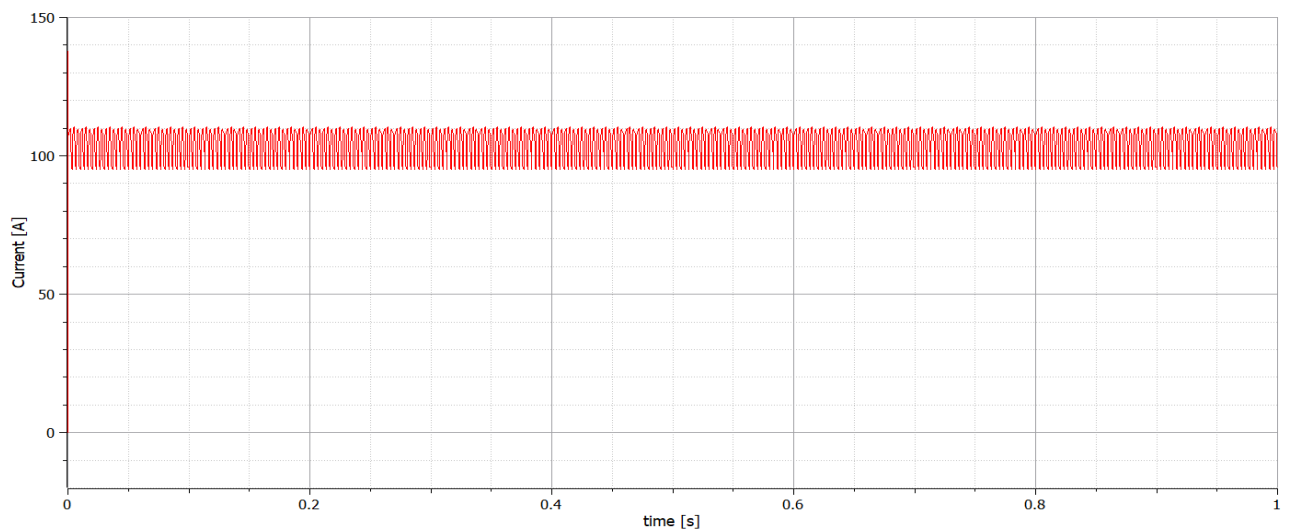


Fig. 6-26: DC current

The batteries are in this case fully charged. State of charge is shown in fig. 6-27:

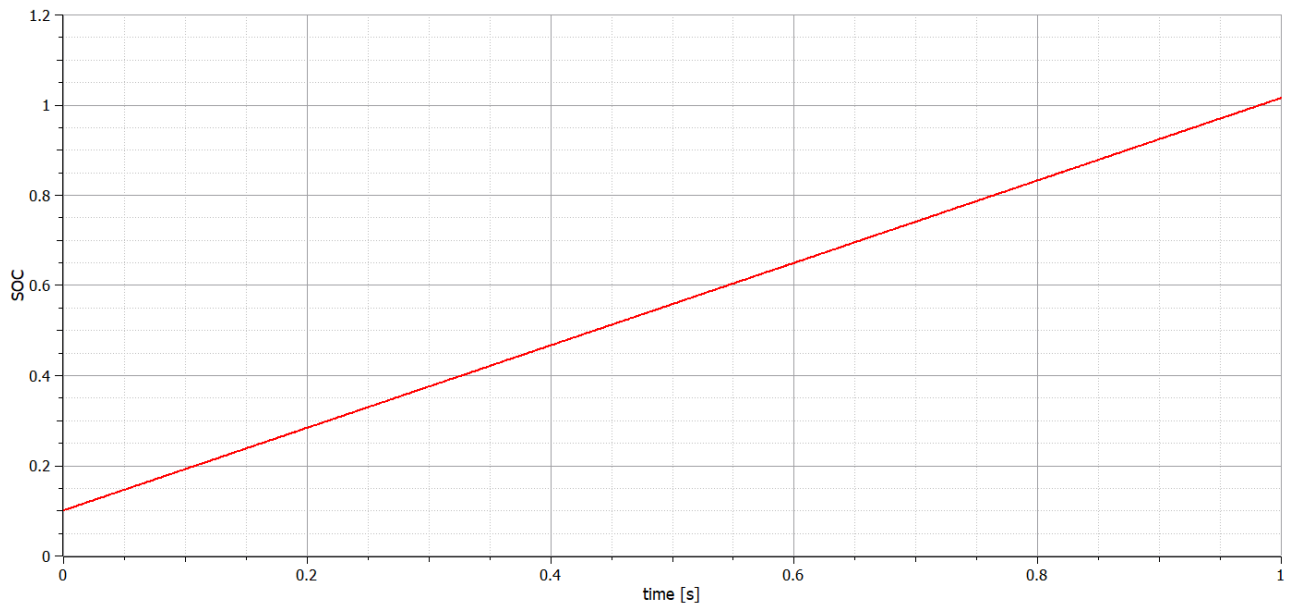


Fig. 6-27: State of charge (SOC)

The energy stored in the batteries is present in fig. 6-28:

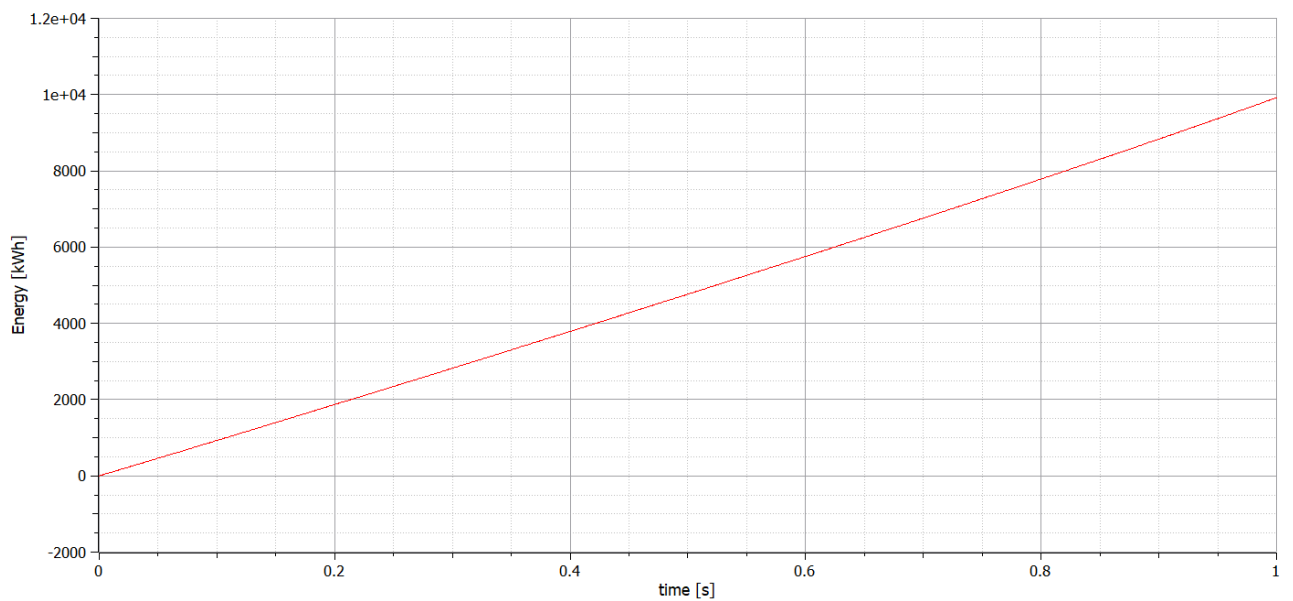


Fig. 6-28: Energy

The efficiency of the system is calculated with the input and output energy. The input energy is that of the 22 kV MV network. $E_{PV} = 11.05$ kWh

$$\eta = \frac{E_{\text{batteries}}}{E_{\text{network}}} = \frac{9.92}{11.05} = 89.8\% \quad (6.38)$$

7 Conclusion

The energy sector has long shifted its focus to renewable energy sources. And with a continuously increasing energy demand, more ways of improving the implementation of renewable sources are emerging. P2G deals with one of renewable energy's main problems, and that is excess production levels due to their fluctuating nature. It presents a new solution in storing electrical energy through converting it to gas.

In P2G, H_2 is produced from water electrolysis. Three types of cells are presented in chapter 2, alkaline, polymer membrane and solid-oxide electrolysis. The three technologies' parameters are listed and compared. AEC and PEMEC are already widely used in commercial projects, while SOEC is still being tested and improved in laboratories. Chapter 3 explains the next step, which deals with CO_2 sources and its feed into the reaction.

The production of SNG in the last step is through methanation. In chapter 4, the methanation reaction is analyzed. The overall reaction is known as Sabatier's reaction. It can be both biological and catalytic, where different types of reactors, as well as various parameters are evaluated for each type. Parameters such as type of catalyst, $H_2:CO_2$ ratio, pressure, temperature, and methanation formation rate.

In the last chapter, the power-to-gas model is presented and analyzed. It includes the production of electricity from a photovoltaic power plant. First, irradiance over the course of a day and the power plant are demonstrated. Next, converting DC to AC, distribution and rectification to output DC current and feed the electrolyzers, and finally electrolysis and methanation. The methanation reaction is solved with van der Waals' equation for real gases. According to that, the production of methane is determined and is then stored in tanks. Furthermore, a simulation is carried out with two paths taken. Firstly, the power gained from the PV power plant is directly converted to feed the electrolyzers. Secondly, the power gained from the PV power plant is fed to the 22 kV MV network, which then powers the rest of the process.

Efficiencies for both cases were determined with the output energy calculated from the heat of combustion of methane. The model with Path 1 had an efficiency of 6.62 % while Path 2 had 8.1 % panels was taken into consideration, enabling the calculation of a more precise efficiency of the system considering the power gained from sunlight. This efficiency was 1.32%. All the calculated efficiencies are in the theoretically expected range. While they are rather low, this is due to power loss over different parts of the process of converting electrical energy into chemical energy. Hydrogen production dominates the losses, but power is also lost in transformers, transmission lines, and methanation. In the battery storage model, efficiencies were relatively high compared to P2G, 64.56 % and 89.8 % for Path 1 and 2 respectively. As for the efficiency including that of the solar panels, it was 12.86 %. This makes battery storage one of the most efficient storage technologies, thus their wide usage in electric vehicles. In P2G, it is still possible to improve the efficiency by utilizing waste heat in electrolysis and methanation.

P2G certainly has a bright future with a lot of room for development. Along with other technologies, P2G helps maintain a more stable power generation ready for higher demands.

References

- [1] World Energy Outlook 2018 [online]. International Energy Agency, 2018 [cit. 2019-10-17]. Available from: <<https://www.iea.org/weo2018/>>
- [2] Global Energy Statistical Yearbook 2019 [online]. Enerdata, 2019 [cit. 2019-10-17]. Available from: <<https://yearbook.enerdata.net/>>
- [3] BP Statistical Review of World Energy 2019 — 68th edition [online]. British Petroleum, 2019 [cit. 2019-10-17]. Available from: <<https://www.bp.com/content/dam/bp/business-sites/en/global/corporate/pdfs/energy-economics/statistical-review/bp-stats-review-2019-full-report.pdf>>
- [4] MAHLIA, T.M.I., T.J. SAKTISAHDAN, A. JANNIFAR, M.H. HASAN and H.S.C. MATSEELAR. A review of available methods and development on energy storage; technology update. *Renewable and Sustainable Energy Reviews*. 2014, 33, 532-545. DOI: 10.1016/j.rser.2014.01.068. ISSN 13640321. Available from: <<https://linkinghub.elsevier.com/retrieve/pii/S1364032114000902>>
- [5] ARGYROU, Maria C., Paul CHRISTODOULIDES and Soteris A. KALOGIROU. Energy storage for electricity generation and related processes: Technologies appraisal and grid scale applications. *Renewable and Sustainable Energy Reviews*. 2018, 94, 804-821. DOI: 10.1016/j.rser.2018.06.044. ISSN 13640321. Available from: <<https://linkinghub.elsevier.com/retrieve/pii/S1364032118304817>>
- [6] ESTERMANN, T., M. NEWBOROUGH and M. STERNER. Power-to-gas systems for absorbing excess solar power in electricity distribution networks. *International Journal of Hydrogen Energy*. 2016, 41(32), 13950-13959. DOI: 10.1016/j.ijhydene.2016.05.278. ISSN 03603199. Available from: <<https://linkinghub.elsevier.com/retrieve/pii/S0360319916317700>>
- [7] GÖTZ, Manuel, Jonathan LEFEBVRE, Friedemann MÖRS, Amy MCDANIEL KOCH, Frank GRAF, Siegfried BAJOHR, Rainer REIMERT and Thomas KOLB. Renewable Power-to-Gas: A technological and economic review. *Renewable Energy*. 2016, 85, 1371-1390. DOI: 10.1016/j.renene.2015.07.066. ISSN 09601481. Available from: <<https://linkinghub.elsevier.com/retrieve/pii/S0960148115301610>>
- [8] THEMA, M., F. BAUER and M. STERNER. Power-to-Gas: Electrolysis and methanation status review. *Renewable and Sustainable Energy Reviews*. 2019, 112, 775-787. DOI: 10.1016/j.rser.2019.06.030. ISSN 13640321. Available from: <<https://linkinghub.elsevier.com/retrieve/pii/S136403211930423X>>
- [9] Power-to-gas industry in Germany to experience massive boost in the next five years [online]. 5.12.2019 [cit. 2020-03-06]. Available from: <<http://www.hydrogenfuelnews.com/power-to-gas-industry-in-germany-to-experience-massive-boost-in-the-next-five-years-8539003/>>

-
- [10] Properties of Hydrogen [online]. Lumen [cit. 2019-10-19]. Available from: <<https://courses.lumenlearning.com/introchem/chapter/properties-of-hydrogen/>>
- [11] Basic Hydrogen Properties Chart [online]. Hydrogen Tools [cit. 2019-10-25]. Available from: <<https://h2tools.org/tools>>
- [12] CHISHOLM, Greig a Leroy CRONIN. Hydrogen From Water Electrolysis. Elsevier, 2016, 2016, , 315-343. DOI: 10.1016/B978-0-12-803440-8.00016-6. ISBN 9780128034408. Available from: <<https://linkinghub.elsevier.com/retrieve/pii/B9780128034408000166>>
- [13] Hydrogen Production: Natural Gas Reforming [online]. Energy.gov [cit. 2019-10-19]. Available from: <<https://www.energy.gov/eere/fuelcells/hydrogen-production-natural-gas-reforming>>
- [14] GAHLEITNER, Gerda. Hydrogen from renewable electricity: An international review of power-to-gas pilot plants for stationary applications. International Journal of Hydrogen Energy [online]. 2013, 38(5), 2039-2061 [cit. 2020-05-24]. DOI: 10.1016/j.ijhydene.2012.12.010. ISSN 03603199. Available from: <<https://linkinghub.elsevier.com/retrieve/pii/S0360319912026481>>
- [15] SCHMIDT, O., A. GAMBHIR, I. STAFFELL, A. HAWKES, NELSON and S. FEW. Future cost and performance of water electrolysis. International Journal of Hydrogen Energy. 2017, 42(52), 30470-30492. DOI: 10.1016/j.ijhydene.2017.10.045. ISSN 03603199. Available from: <<https://linkinghub.elsevier.com/retrieve/pii/S0360319917339435>>
- [16] Hydrogen transport & distribution [online]. Hydrogen Europe, 2017 [cit. 2019-11-16]. Available from: <<https://hydrogeneurope.eu/hydrogen-transport-distribution/#Compressed>>
- [17] BP Energy Outlook 2019 edition. British Petroleum [online]. London, United Kingdom: British Petroleum, 2019 [cit. 2019-10-27]. Available from: <<https://www.bp.com/content/dam/bp/business-sites/en/global/corporate/pdfs/energy-economics/energy-outlook/bp-energy-outlook-2019.pdf>>
- [18] REITER, Gerda and Johannes LINDORFER. Evaluating CO₂ sources for power-to-gas applications – A case study for Austria. Journal of CO₂ Utilization. 2015, 10, 40-49. DOI: 10.1016/j.jcou.2015.03.003. ISSN 22129820. Available from: <<https://linkinghub.elsevier.com/retrieve/pii/S2212982015000244>>
- [19] POST-COMBUSTION CO₂ CAPTURE [online]. National Energy Technology Laboratory [cit. 2019-11-02]. Available from: <<https://www.netl.doe.gov/coal/carbon-capture/post-combustion>>
- [20] PRE-COMBUSTION CO₂ CAPTURE [online]. National Energy Technology Laboratory [cit. 2019-11-02]. Available from: <<https://www.netl.doe.gov/coal/carbon-capture/pre-combustion>>

- [21] VASUDEVAN, Suraj, Shamsuzzaman FAROOQ, Iftekhar A. KARIMI, Mark SAEYS, Michael C.G. QUAH a Rakesh AGRAWAL. Energy penalty estimates for CO₂ capture: Comparison between fuel types and capture-combustion modes. *Energy*. 2016, 103, 709-714. DOI: 10.1016/j.energy.2016.02.154. ISSN 03605442. Available from: <<https://linkinghub.elsevier.com/retrieve/pii/S036054421630216X>>
- [22] GHAIB, Karim and Fatima-Zahrae BEN-FARES. Power-to-Methane: A state-of-the-art review. *Renewable and Sustainable Energy Reviews*. 2018, 81, 433-446. DOI: 10.1016/j.rser.2017.08.004. ISSN 13640321. Available from: <<https://linkinghub.elsevier.com/retrieve/pii/S1364032117311346>>
- [23] HARKIN, Trent, Andrew HOADLEY and Barry HOOPER. Reducing the energy penalty of CO₂ capture and compression using pinch analysis. *Journal of Cleaner Production*. 2010, 18(9), 857-866. DOI: 10.1016/j.jclepro.2010.02.011. ISSN 09596526. Available from: <<https://linkinghub.elsevier.com/retrieve/pii/S0959652610000491>>
- [24] MEYER, Leo, METZ, Bert, Ogunlade DAVIDSON, Heleen DE CONINCK and Manuela LOOS, ed. CARBON DIOXIDE CAPTURE AND STORAGE. Geneva, Switzerland: Cambridge University Press. Published for the Intergovernmental Panel on Climate Change, 2005, , 4. Available from: <https://www.ipcc.ch/site/assets/uploads/2018/03/srccs_wholereport-1.pdf>
- [25] Carbon Dioxide Emissions Associated with Bioenergy and Other Biogenic Sources [online]. United States Environmental Protection Agency [cit. 2019-11-08]. Available from: <https://19january2017snapshot.epa.gov/climatechange/carbon-dioxide-emissions-associated-bioenergy-and-other-biogenic-sources_.html>
- [26] How Carbon Capture Works [online]. HowStuffWorks.com, 2008 [cit. 2019-11-16]. Available from: <<https://science.howstuffworks.com/environmental/green-science/carbon-capture2.htm>>
- [27] CHANDEL, Munish and Eric WILLIAMS. Synthetic Natural Gas (SNG):Technology, Environmental Implications, and Economics. Duke, Nicholas Institute [online]. North Carolina, USA: Nicholas Institute, Duke University, 2009 [cit. 2019-11-09]. Available from: <<https://nicholasinstitute.duke.edu/sites/default/files/publications/natgas-paper.pdf>>
- [28] STANGELAND, Kristian, Dori KALAI, Hailong LI and Zhixin YU. CO₂ Methanation: The Effect of Catalysts and Reaction Conditions. *Energy Procedia*. 2017, 105, 2022-2027. DOI: 10.1016/j.egypro.2017.03.577. ISSN 18766102. Available from: <<https://linkinghub.elsevier.com/retrieve/pii/S187661021730629X>>
- [29] HOEKMAN, S. Kent, Amber BROCH, Curtis ROBBINS and Richard PURCELL. CO₂ recycling by reaction with renewably-generated hydrogen. *International Journal of Greenhouse Gas Control*. 2010, 4(1), 44-50. DOI: 10.1016/j.ijggc.2009.09.012.

- ISSN 17505836. Available from: <<https://linkinghub.elsevier.com/retrieve/pii/S1750583609001005>>
- [30] GAO, Jiajian, Yingli WANG, Yuan PING, Dacheng HU, Guangwen XU, Fangna GU and Fabing SU. A thermodynamic analysis of methanation reactions of carbon oxides for the production of synthetic natural gas. *RSC Advances*. 2012, 2(6). DOI: 10.1039/c2ra00632d. ISSN 2046-2069. Available from: <<http://xlink.rsc.org/?DOI=c2ra00632d>>
- [31] BECKER, William L., Michael PENEV and Robert J. BRAUN. Production of Synthetic Natural Gas From Carbon Dioxide and Renewably Generated Hydrogen: A Techno-Economic Analysis of a Power-to-Gas Strategy. *Journal of Energy Resources Technology*. 2019, 141(2). DOI: 10.1115/1.4041381. ISSN 0195-0738. Available from: <<https://asmedigitalcollection.asme.org/energyresources/article/doi/10.1115/1.4041381/474624/Production-of-Synthetic-Natural-Gas-From-Carbon>>
- [32] EIGENBERGER, GERHART. Fixed-Bed Reactors [online]. Institut für Chemische Verfahrenstechnik, Universität Stuttgart, Stuttgart, Federal Republic of Germany [cit. 2019-11-09]. Available from: <<https://elib.uni-stuttgart.de/bitstream/11682/1848/1/eig16.pdf>>
- [33] KOPYSCINSKI, Jan, Tilman J. SCHILDHAUER and Serge M.A. BIOLLAZ. Methanation in a fluidized bed reactor with high initial CO partial pressure: Part I—Experimental investigation of hydrodynamics, mass transfer effects, and carbon deposition. *Chemical Engineering Science*. 2011, 66(5), 924-934. DOI: 10.1016/j.ces.2010.11.042. ISSN 00092509. Available from: <<https://linkinghub.elsevier.com/retrieve/pii/S0009250910007049>>
- [34] YOUNAS, Muhammad, Leong LOONG KONG, Mohammed J. K. BASHIR, Humayun NADEEM, Areeb SHEHZAD and Sumathi SETHUPATHI. Recent Advancements, Fundamental Challenges, and Opportunities in Catalytic Methanation of CO₂. 2016, 30(11), 8815-8831. DOI: 10.1021/acs.energyfuels.6b01723. ISSN 0887-0624. Available from: <<https://pubs.acs.org/doi/10.1021/acs.energyfuels.6b01723>>
- [35] TODIĆ, Branislav, Vitaly V. ORDOMSKY, Nikola M. NIKAČEVIĆ, Andrei Y. KHO-DAKOV and Dragomir B. BUKUR. Opportunities for intensification of Fischer–Tropsch synthesis through reduced formation of methane over cobalt catalysts in microreactors. 2015, 5(3), 1400-1411. DOI: 10.1039/C4CY01547A. ISSN 2044-4753. Available from: <<http://xlink.rsc.org/?DOI=C4CY01547A>>
- [36] LEFEBVRE, Jonathan, Manuel GÖTZ, Siegfried BAJOHR, Rainer REIMERT and Thomas KOLB. Improvement of three-phase methanation reactor performance for steady-state and transient operation. *Fuel Processing Technology*. 2015, 132, 83-90. DOI: 10.1016/j.fuproc.2014.10.040. ISSN 03783820. Available from: <<https://linkinghub.elsevier.com/retrieve/pii/S0378382014004640>>

-
- [37] OMEdit – OpenModelica Connection Editor [online]. openmodelica.org, 2017 [cit. 2020-03-31]. Available from: <<https://openmodelica.org/doc/OpenModelicaUsersGuide/v1.11.0/omedit.html>>
- [38] SHARP NU Series 185 W —180 W: Monocrystalline silicon photovoltaic modules [online]. SOLAR ACCESS [cit. 2020-05-25]. Available from: <<https://planning.islington.gov.uk/NorthgatePublicDocs/00185345.pdf>>
- [39] IV Curve. PVEducation [online]. 2019 [cit. 2020-05-15]. Available from: <<https://www.pveducation.org/pvcdrom/solar-cell-operation/iv-curve>>
- [40] Overhead Line (OHL) Electrical Parameters [online]. [cit. 2020-06-03]. Available from: <https://www.powerwiki.cz/attach/PPE/PPE_pr02_parametry.pdf>
- [41] Three Phase Rectification [online]. Electronics Tutorials [cit. 2020-06-01]. Available from: <https://www.electronics-tutorials.ws/power/three-phase-rectification.html>
- [42] VÁVRA, Robert. Model energetického systému s vodíkovou akumulací [online]. Brno, 2019 [cit. 2020-05-14]. Available from: <<https://www.vutbr.cz/studenti/zav-prace/detail/115671>>.
- [43] Van der Waals Equation [online]. [cit. 2020-04-13]. Available from: <<https://courses.lumenlearning.com/introchem/chapter/van-der-waals-equation/>>
- [44] Real Gases - Van der Waals Equation [online]. [cit. 2020-04-13]. Available from: <http://www.molecularsoft.com/help/Gas_Laws-Real_Gas.htm>
- [45] Zemní plyn - spalné teplo a další vlastnosti: Spalné teplo, výhřevnost, energetická hustota, Wobbeho číslo, stechiometrický poměr a přebytek vzduchu [online]. TZB-info, 30.4.2004 [cit. 2020-05-22]. Available from: <<https://vytapani.tzb-info.cz/vytapime-plynem/1963-spalovaci-vlastnosti-zp-i>>
- [46] Spalné teplo. Wikipedia [online]. 15. 6. 2019 [cit. 2020-05-15]. Available from: <https://cs.wikipedia.org/wiki/Spaln%C3%BD_teplo>